www.saltworkconsultants.com

Salty Matters

John Warren -Thursday October 31, 2019

Saline Dolomites: Ancient - Part 4 of 4 - Saddle dolomite, calcite and anhydrite spar burial salts

Introduction

Large volumes of ancient saline dolomites not only precipitate as eogenetic brine reflux dolomites (part 3 of this series of four articles on dolomite) but can also form in the relatively warm burial environments characterising the mesogenetic realm, especially regions of saline basinal waters, in fault-fed regions often tied to dissolving evaporites. In this context saddle dolomite is considered an archetypal burial carbonate precipitated from hot saline basinal fluids. Some saddle dolomite precipitates are intimately associated with a range of indicators of thermally altered evaporite salts, especially burial anhydrite spar, others are not. Later, I will emphasise the burial anhydrite association, but first I will take a more conventional path by presenting a consensus discussion of what is known more generally about the significance of saddle dolomite occurrences in sedimentary basins

Saddle dolomite is a hydrothermal mineral

There are three main products created by the hydrothermal fluid invasion of a carbonate host: 1) saddle dolomite (a burial dolomite), 2) leached limestone ("hydrothermal karst"), and 3) sulphide minerals, particularly galena and sphalerite. Saddle dolomite is considered one of the key indicators of saline hydrothermal fluid involvement in mesogenetic diagenesis (Du et al., 2018; Davies and Smith, 2006; Spötl and Pitman, 1998; Radke and Mathis, 1980). Saddle dolomite can, however, be absent in a hydrothermal deposit, and saddle dolomite can occur in strata not influenced by hydrothermal crossflows. So, the current geological consen-

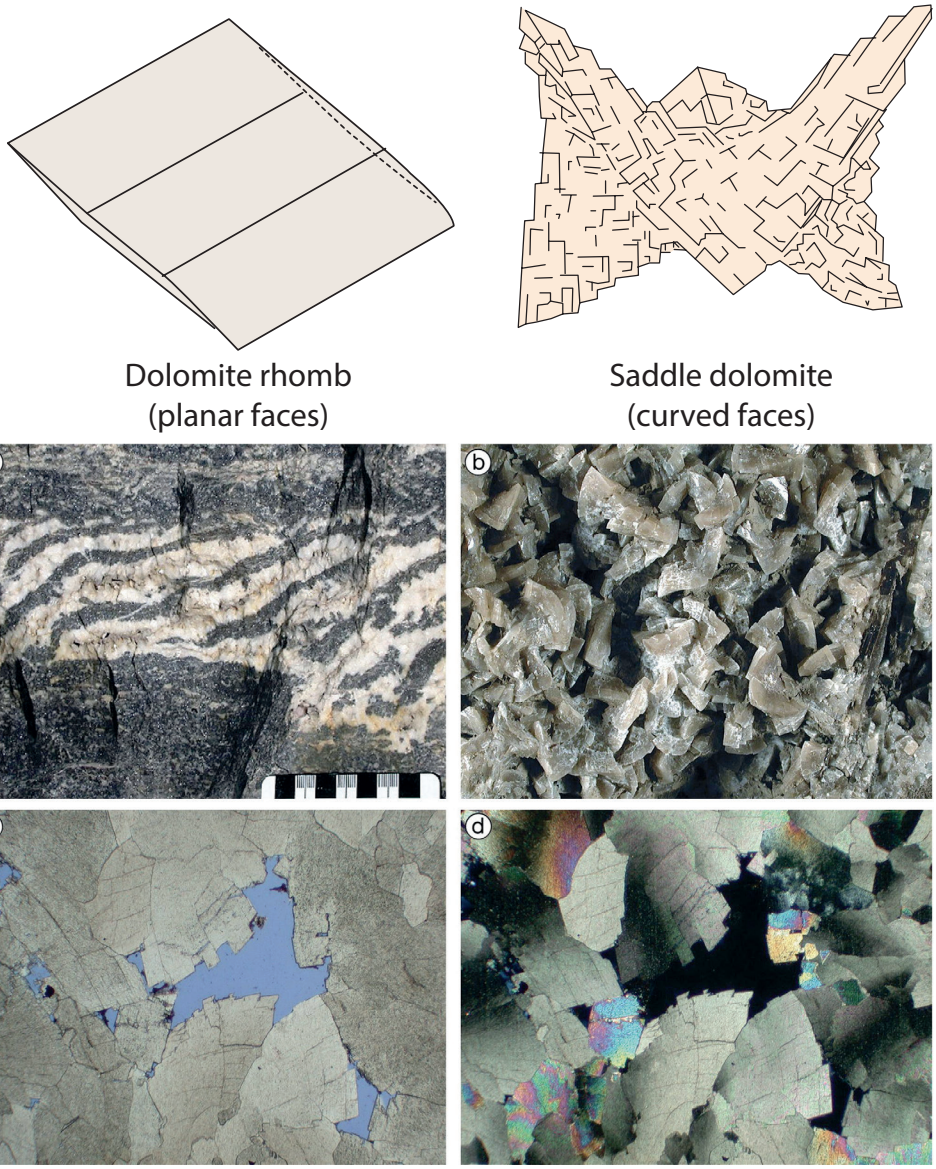

Figure 1. Dolomite morphologies - rhomb versus saddle, with saddle dolomite examples (courtesy of Noel James) A) Zebra dolomite hydrofractures with white sparry saddle dolomite in pores (Upper Cambrian, Alberta). B) Sparry dolomite pore fill, core Devonian Canada (image is 3 cm wide). C) Close-up of curved crystal faces that typify saddle dolomites (blue is porosity (epoxy impregnated - photomicrograph taken in non-polarised light, image is 2 cm wide. D) same view as C but using crossed polars showing typical sweeping or undulasoe extinction.

sus is that its presence is not always diagnostic of a hydrothermal interaction.

Saddle dolomites's most common modes of occurrence are either (1) as coarse void fill cement or (2) as coarse replacements in precursor matrices of limestone or dolomite (Moore, 2009). The replacement mode is the most volumetrically and economically significant style in hydrocarbon reservoirs and is often tied to the development of vuggy porosityalong with interconnection via polyhedral pores within the matrix.

As indicated by its name, saddle dolomite is characterised by curved crystal faces and undulose or sweeping extinction in crossed polarised light (Figure 1). Crystals tend to be white or buff rather than transparent due to numerous brine inclusions (Figure 1a,b). Thermal analysis of the inclusions indicate saddle dolomite precipitates in relatively warm subsurface waters (80–180 °C), while inclusion chemistries indicate $MgCl_2$–$CaCl_2$–NaCl–H_2O basinal brine parentages, with salinities generally 4-8 times that of seawater (Figure 2c). Davies and Smith (2006) attribute the elevated salinities to a post-evaporite dissolution source that is variably modified by mixing with seawater or freshwater, and by deep burial interaction with basement or siliciclastic rocks. Saddle dolomites tend to have elevated radiogenic strontium values, suggesting fluid sources that have interacted with siliciclastics or basement rocks. ^{18}O values tend to be depleted, also consistent with a higher temperature origin.

According to one of the earlier papers discussing the likely reason for the characteristic curved crystal faces, Radke and Mathis (1980) argue for the preferential insertion of Ca distorting the crystal lattice. Saddle dolomites are slightly enriched in calcium with significant variations in composition within individual growth laminae. Calcium is more abundant in the lattice at crystal apices and face edges that are at higher angles to the 'c' axis, than towards face centres. These composition gradients along growth laminae cause the lattice distortion, which has trigonal symmetry corresponding to the saddle morphology. The cause of selective ion adsorption during crystal growth is open to speculation but must be associated with the crystal as an entity. Surface-charge effects, the most probable cause, may be produced by either a pyroelectric phenomenon at elevated temperatures or pH and ionic concentrations of the precipitating fluids.

Wendte et al. (1998), Morrow et al. (2002), and Saller and Dickson (2001) suggested that hypersaline evaporite-residual brines were responsible for the hydrothermal saddle dolomite reservoirs they studied in the Western Canada Sedimentary and Midland basins. Du et al. (2018) suggested a similar post-evaporite association for the saddle dolomites in the Tahe oilfield of the Tarim Basin, China. Saddle dolomites that typify some MVT basins, such as the Silurian-hosted ores in the Cadjebut Region in the Canning Basin of West Australia, precipitate from chloride-rich basinal brines created by the dissolution of deeply buried halite (Kempton and Warren, 1998). Metal fixation occurs higher in the stratigraphy at TSR sites tied to bedded calcium sulphate beds and faulted hydrocarbon traps (Wallace et al., 1997; Warren, 2016).

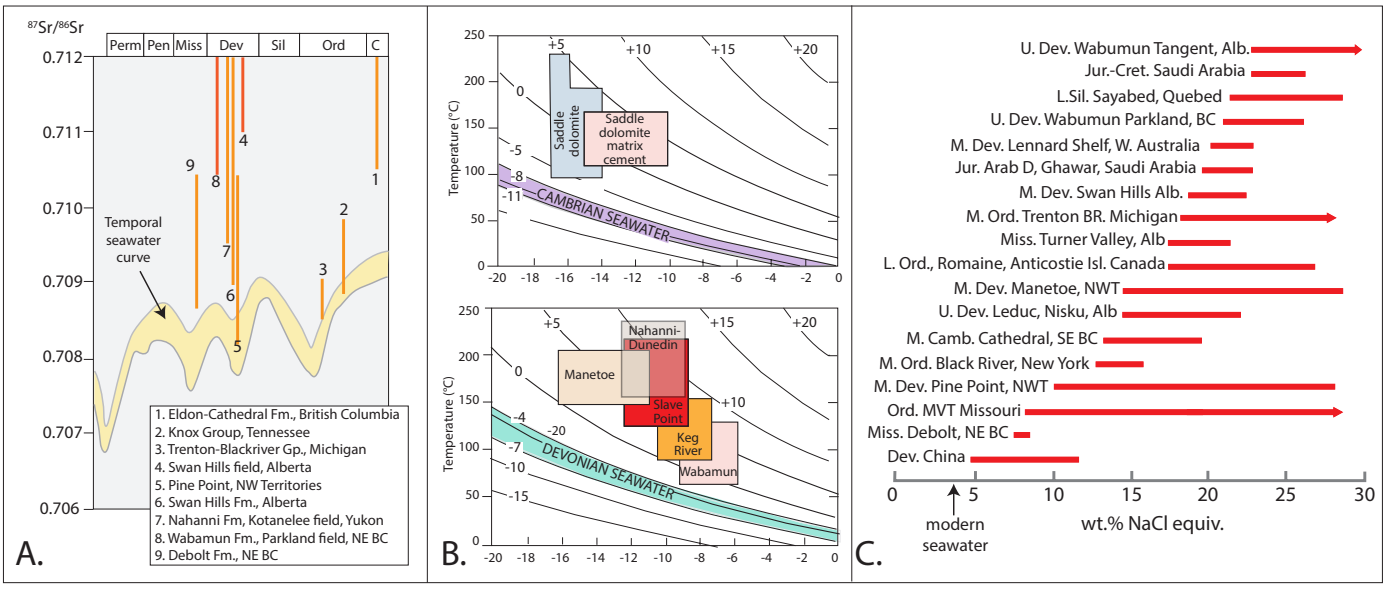

Figure 2. Geochemical characterisation of Saddle Dolomite (in part after Davies and Smith, 2006). A) $^{87}Sr/^{86}Sr$ isotopic composition of saddle dolomite from selected Paleozoic host locations in western Canada and the eastern United States, plotted relative to the global temporal seawater strontium curve. The plot shows that saddle dolomite in Cambrian, Ordovician, Devonian, and Mississippian hosts is near-universally enriched in the radiogenic isotope of strontium. The source of radiogenic strontium may be from saline siliciclastic aquifers, but the more highly elevated radiogenic signatures may indicate a basement source. B) Crossplots of fluid-inclusion homogenization temperature (Th) against oxygen isotopic signature for matrix-replacive and void-filling saddle dolomite from outcrop and subsurface locations in the Cambrian and the Devonian of western Canada. Cambrian data are from the Cathedral and Eldon formations exposed in southeastern British Columbia and southwestern Alberta. Contours are for the isotopic composition of water in isotopic equilibrium with the dolomite. Both plots show that dolomite formed from water enriched to strongly enriched in $\delta^{18}O_{PDB}$ compared with the estimated isotopic composition of contemporaneous seawater; this relationship is typical of hydrothermal systems. C) Bar plot showing ranges of salinity in two-phase fluid inclusions in saddle dolomite, based on the melting point temperature (Tm) of ice, from selected western Canadian and global locations. Most values are more than three times the salinity of modern seawater, to more than eight times. I have plotted from the base in increasing order from the lowest salinity value.

Davies and Smith (2006) also cite several cases where dissolving evaporites are the probable ultimate source for dolomitizing brines, but also discuss examples where no evaporites were involved. In the latter case, a magmatic source is generally needed to supply sufficient Mg for dolomitisation. In rift basins that lack an evaporitic (halite) base level in the basin stratigraphy, magmatic fluid interactions offer a viable Mg source to explain saddle dolomite - porosity associations. Due to elevated acidity, magmatically-sourced brines are chemically likely to be highly aggressive toward limestones, as are thermochemical sulphate reduction brines (Moore, 2009; Warren, 2016).

Leached limestones form in a range of hydrothermal settings, because of the retrograde solubility of calcite and the generally acidic nature of hydrothermal fluids (Davies and Smith, 2006; Heydari, 1997). Hence limestone and evaporite leaching is likely where hydrothermal fluids move up a fault and come into contact with cooler limestones and evaporites at shallower depths. There, significant amounts of secondary porosity can form, particularly in facies like grainstones with relict porosity, or intervals characterised by the dissolution of prograde salts such as halite cements or evaporite-dissolution associated aquifers. If a sufficient volume of limestone or soluble evaporite is removed, the leached section is termed a hydrothermal karst (Loucks, 1999).

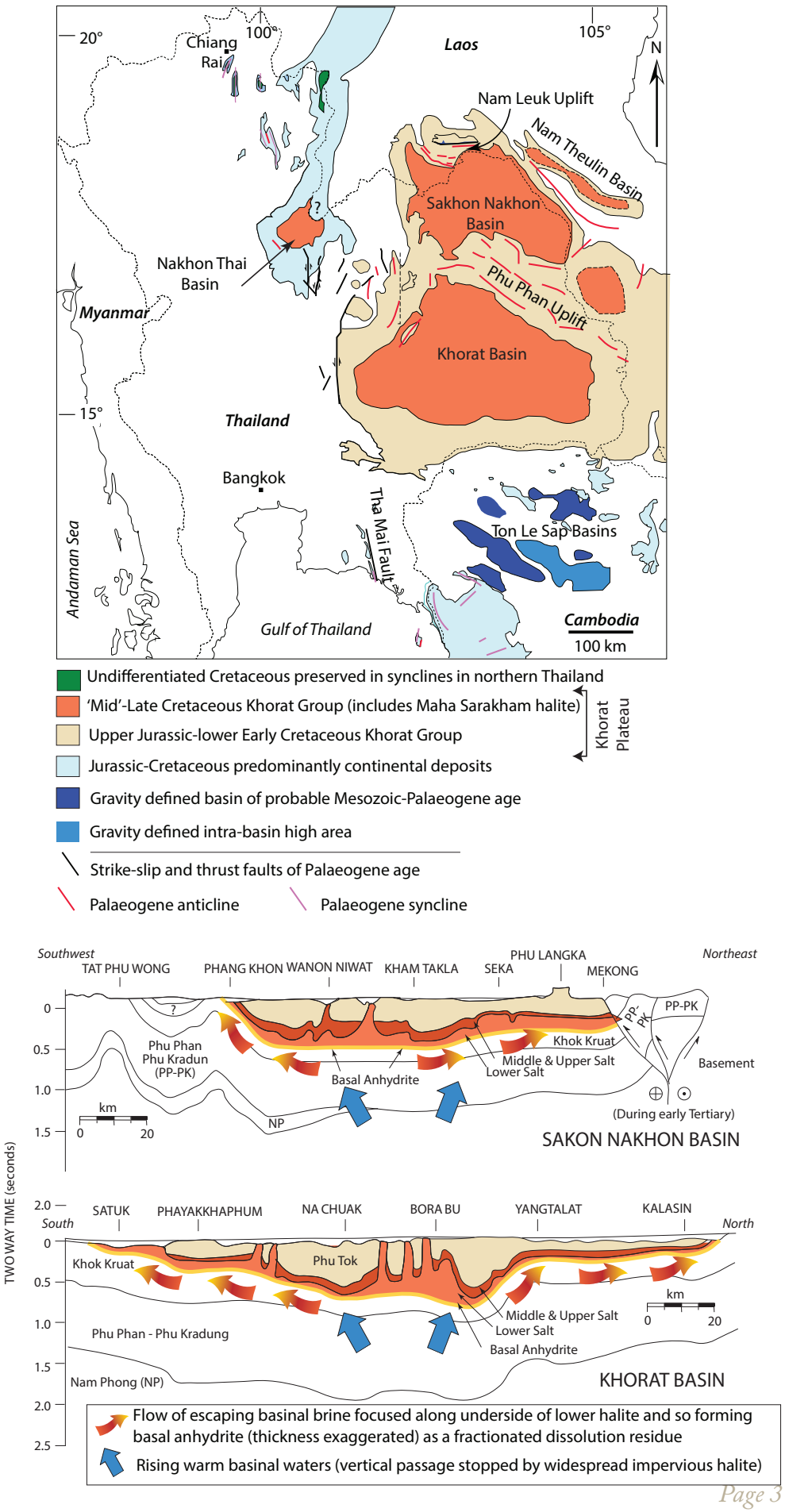

Figure 3. General Geology of the Khorat Basin in Thailand and surrounds (after Morley et al. 2012 and Warren, 2016). The basal anhydrite accretes diagenetically as basinal water flow is focused along the underbelly of the impervious lower halite. Convecting (density and thermal drive) basinal waters, along with compactional waters, circulate through a 5-km-thick sequence of nonmarine and feldspathic red beds that underlie the Maha Sarakham evaporites. The Basal Anhydrite forms in the zone of contact between upwelling cells of these basinal waters and the dissolving underside of the halite evaporites.

The remainder of this article focuses on occurrences of basinal precipitation of saddle dolomite where evaporite mesogenetic salts such as sparry anhydrite and burial halite cements, or evaporite dissolution breccias and other evaporite indicator textures are also present.

Saddle dolomite - evaporite association

To discuss precipitative mechanisms and the association of saddle dolomite with burial evaporites, occurrences are divided into examples where; 1) the saddle dolomite is encased in anhydrite, 2) saddle dolomite crystals form along with burial anhydrite (and its destruction) in regions of thermochemical sulphate reduction (TSR), 3) where the saddle dolomites occurs in a variety of MVT deposits in proximity to sparry anhydrite or other saline burial indicators.

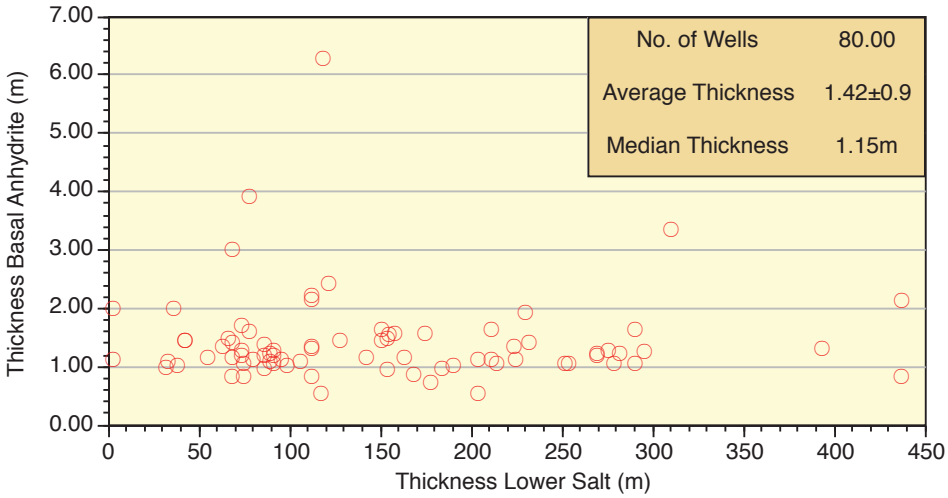

Figure 4. Crossplot of thickness of the basal anhydrite unit versus thickness of the overlying "Lower Salt" in the Maha Sarakham Formation, Thailand (after Warren, 2016).

Saddle dolomite is encased in diagenetic anhydrite

Gypsum-anhydrite caprocks atop diapirs are widely recognised products of preferential salt dissolution. Less widely recognised stratiform equivalents to caprocks occur where undersaturated groundwaters flush the upper and lower contacts of stratiform or bedded halite. Such a set of processes affects halite beds in Maha Sarakham evaporites beneath the Khorat Plateau of NE Thailand (Figure 3; Warren 2016, Chapter 7 for details). Preferential dissolution of the underside of the Maha Sarakham Formation of NE Thailand is occurring where the underbelly of the halite is bathed in a crossflow of compactional and thermobaric waters (Figure 3; Warren 1997; El Tabakh et al., 1998). The resulting basal anhydrite passes downward, via a thin cm-thick organic-rich residue layer, into underlying nonevaporite sediment made up of calcite-cemented fluvial sands and shales of the Khok Kruat Group.

To document the subsurface processes that alter the underside of thick evaporite beds, the salt units of the Khorat Plateau of NE Thailand are ideal (Figure 3). The region is unique in that the various salt layers of the Maha Sarakham Formation have been extensively and continuously cored from top to bottom, and a simple gamma log suite run in the boreholes. This was done in the 1970s and 1980s in a World Bank-funded exploration project for potash salts. The cores were double-sealed in plastic wrap and archived at a DMR core store in Udon Thani, where they are still available for study.

Everywhere it was cored, the underside of the thick Lower Salt of the Maha Sarakham Formation is typified by a thin, distinc-

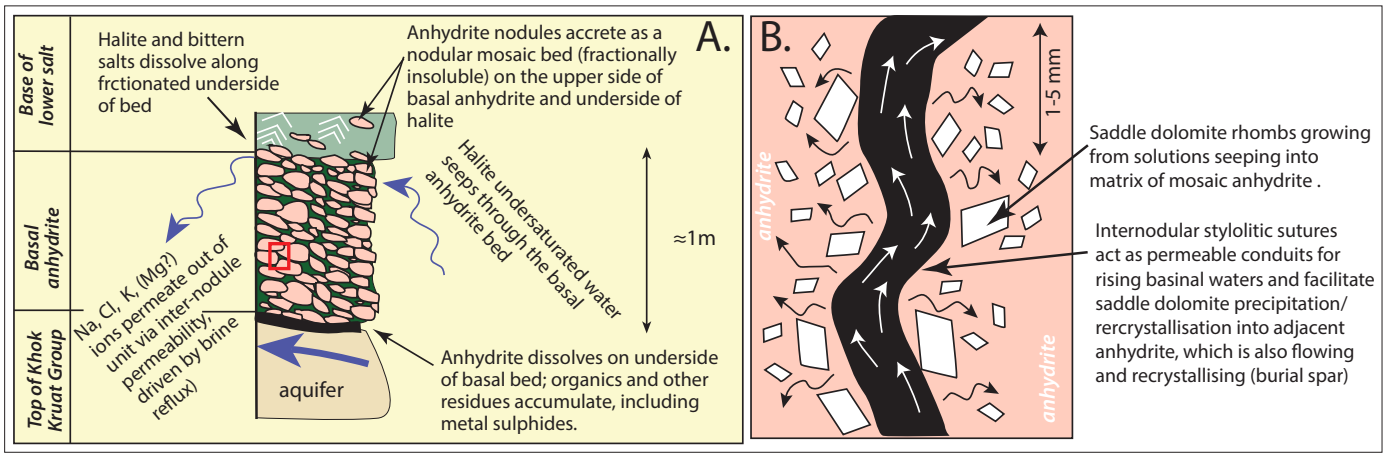

Figure 5. Formation and geochemical character of the basal anhydrite (after El Tabakh, 1998, 2003; Warren 2016). A) Schematic model of the base of the Maha Sarakham Formation where the basal contact of the Maha Sarakham evaporite sequence is a site of fluid flushing from below. It is characterised by halite dissolution, anhydrite recrystallisation into coarse and sparry anhydrite and the growth of saddle dolomite in the recrystallised anhydrite (see Figure 6). B) Enlarged view of position shown by red rectangle in Figure 5a. At the same time as fractionating dissolution and recrystallisation of anhydrite is occurring in the basal anhydrite, coarsely crystalline and saddle dolomite is precipitated, recrystallised and isotopically modified into various coarse and saddle crystals adjacent to active stylolitic inter-anhydrite nodule sutures (black area in the middle of the figure). These inter-nodule stylolitic sutures are permeable and facilitate the passage of the brines that carry the ions precipitated as the coarse and saddle dolomites, while at the same time take away the dense refluxing chloride brines created by halite dissolution at the upper side of the basal anhydrite unit. Hence, there is a general decrease in dolomite rhomb sizes away from the stylolite conduits.

tive basal anhydrite bed composed of flattened mosaic nodules, with a bed thickness that is surprisingly consistent; averaging 1.42 metres (Figure 4).

The basal anhydrite is a diagenetic unit created by ongoing salt dissolution. It is a pressure-welded nodular anhydrite unit, accreted in the subsurface as a widespread buildup of relatively insoluble anhydrite residues on the underside of a dissolving halite sequence (Figure 5a). Fractional dissolution is driven by the escape of undersaturated compactional and thermobaric waters. It is, in effect, an upside-down caprock (Figure 5; El Tabakh et al., 1998; Warren 2016). That is, the basal anhydrite defines the regional diagenetic underside of the variable-halokinetic salt beds of the Cretaceous Maha Sarakham Formation of Thailand (Figure 3). Its self-limiting transmissivity means the basal anhydrite bed is characterised by a near-constant basinwide thickness, and consistent stratigraphic textures across the underside of large portions of the salt (Figure 4). In many evaporite basins of the world, similar constant-thickness beds are also called basal anhydrites, but are assigned a primary depositional origin.

The near-constant thickness of the basal anhydrite across the Khorat and Sakon Nakhon basins reflects the intrinsic self-limiting permeability of a nodular anhydrite unit accreting diagenetically beneath a salt overburden. Wherever upwelling basinal waters contact the underside of the Lower Salt unit, it dissolves fractionally, leaving behind a nodular anhydrite residue. The nodular residue continues to accrete along its top by gathering anhydrite nodules via the preferential solution of halite. Nodules were initially suspended within the now dissolving bedded halite. At the same time, as new nodules are accreting along the upper side of the basal anhydrite, the anhydrite is dissolving along its underside (Figure 5).

The overall dissolution process is driven by escaping compactional waters flushing the underbelly of the salt. If the basal anhydrite accretes to where it is more than a metre or two thick, it starts to act as an aquitard for waters seeping through its internodular porosity. This slows water access to the halite contact. Thickness of the basal anhydrite can increase until it reaches a point where undersaturated compactional waters can no longer flow through internodule permeability to reach the halite-anhydrite dissolution front. Once undersaturated waters no longer access the halite dissolution front, anhydrite accretion slows and even shuts down along the upper side of the basal anhydrite unit. Even so, compacting undersaturated waters continue to flow along the underside of the basal anhydrite, where anhydrite dissolution occurs. Once sufficient anhydrite dissolves from its underside, undersaturated waters can again reach the halite and dissolve it anew. Basinwide near-constant thickness of the basal anhydrite reflects a buffering interaction between the rate of anhydrite nodule accretion or docking on its upper surface and the rate of anhydrite loss on its lower surface. In effect, a basal anhydrite has a "half-life." The actual thickness of the basal anhydrite is determined by the inherent transmissivity of the material between the nodules.

Unlike depositional anhydrites within saline giant fills, which typically thicken into the lowstand platform wedge, the mesogenetic flow-controlled diagenetic origin of the basal anhydrite of the Maha Sarakham creates a diagnostic near-constant thickness across the entire basin that is independent of the thickness of the overlying salt. There are a few wells where the anhydrite is thicker than 1-2 metres, but there the anhydrite shows evidence of flow thickening and the wells are typically located at or near the dissolution edge of the Lower Salt where larger karst cavities can form, and suprasalt and subsalt sulphate residues can fold, fault and stack (Warren, 2016; Chapter 7)

The basal anhydrite contains numerous mesogenetic saddle and coarsely crystalline dolomites encased in nodular anhydrite (Figure 6). These burial-stage coarse and saddle calcian dolomites precipitate from the same rising basinal brines that are dissolving the underside of the halite and creating the basal anhydrite. Saddle dolomites in the Basal Anhydrite Unit are characterized by (Figure 6): (a) coarse crystals that average 1.5 mm, (b) subhedral to euhedral crystal shapes, (c) a lack of replacement textures or other evidence of any precursor carbonate, (d) abundant inclusions, (e) an association with stylolites and coarse, sparry and

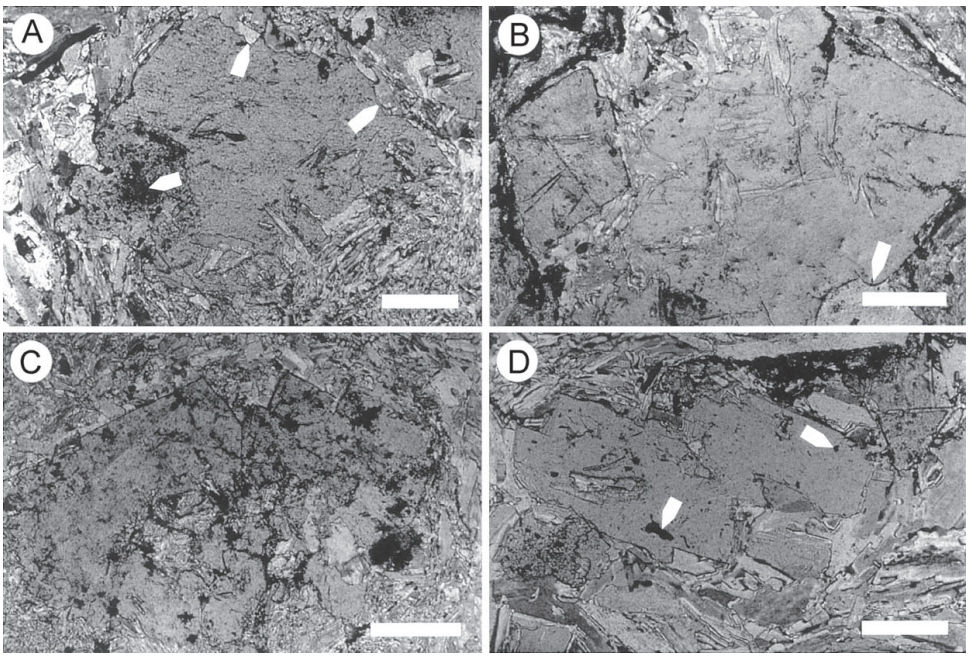

Figure 6. Petrology of the saddle dolomite in the Basal Anhydrite Unit (after El Tabakh et al., 2003). (A) Photomicrograph of a subhedral dolomite crystal with numerous dark, fluid inclusions found within recrystallized anhydrite (arrow points to left) and irregular crystal rims (two other arrows). Scale bar is 0.5 mm. (B) Very coarse saddle dolomite crystal that almost fills the field of view with minor laths of anhydrite inclusions. Some of the crystal edges are curved (at arrow). Scale bar is 0.5 mm. (C) A group of subhedral dolomite crystals forming typical saddle-shape forms. The lower parts of the crystals are marked by stylolites. Scale bar is 0.5 mm. (D) A lcoarsely crystalline, subhedral dolomite crystal found 'floating' in anhydrite mass. Arrows point to fluid inclusions. Scale bar is 0.5 mm.

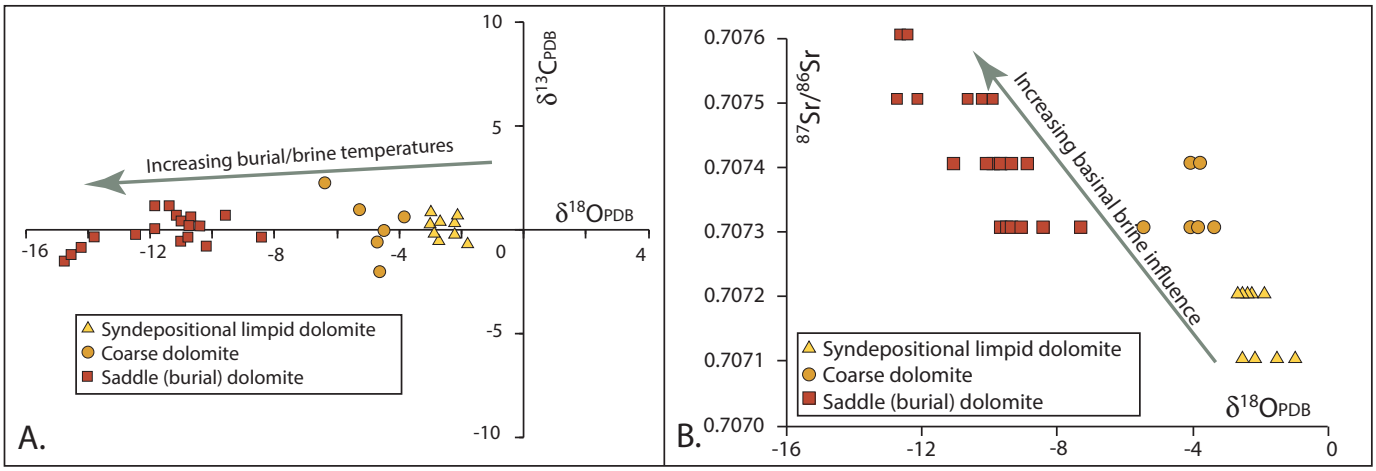

Figure 7. A) δC_{PDB}-δO_{PDB} isotopic signatures in the three types of dolomite occurring in the basal anhydrite of the Maha Sarakham Fm. Thailand showing influence of increasing temperature related to ongoing burial. B) Crossplot of $\delta^{18}O_{PDB}$ versus $^{87}Sr/^{86}Sr$ showing influence of ongoing basin brine evolution from limpid dolomite through coarse and saddle dolomite precipitates (after el Tabakh et al., 2003.

recrystallized anhydrite, and (f) euhedral crystals that are individual, free growth forms lacking sutured contacts. They exhibit characteristic curved surfaces and weak sweeping extinction. These petrographic features clearly separate them morphologically from the coarse, subhedral to euhedral dolomites. Generally, the saddle dolomite crystals are unimodal, with nonplanar textures and nearly equant outlines.

Saddle dolomite in the basal anhydrite is intimately associated with the more-intensely recrystallized coarsely-crystalline anhydrite. The latter is made up of large, poorly-oriented, elongated laths of sparry and blocky crystals up to 5-mm size. In core, the saddle dolomite crystals are white, except where they contain fewer inclusions (Figure 6a). The larger saddle dolomite crystals have irregular crystal rims near the contact with the surrounding anhydrite. They may contain inclusions of anhydrite, implying poikiliotopic growth of the dolomite into a milieu of recrystallising anhydrite (Figure 6b). Some saddle dolomite crystals contain numerous small fluid inclusions (Figure 6a, c). Locally, the dolomite crystals show subhedral shapes and irregular crystal edges (Figure 6d) that define stylolitic zones (Figure 6b, c)). Similar large and euhedral saddle dolomite crystals are also present as intergranular cements and over-growths on sandstone grains in the uppermost section of the underlying Khok Kruat Formation indicating that saddle dolomite-forming fluids also penetrated the upper part of the underlying sandstone. Saddle dolomite does not occur in the precursor halite beds.

Saddle dolomite crystals have $\delta^{18}O_{PDB}$ values that range from -8.2‰ to -14.2‰ and $\delta^{13}C_{PDB}$ values that range from +1.8‰ to -1.9‰ (Figure 7a). Like the associated coarse dolomite, the $^{87}Sr/^{86}Sr$ ratios of the saddle dolomites range from 0.70771 to 0.7076 and so are mostly more radiogenic (basement-derived) compared to Cretaceous-age, marine dolomites with values around 0.70745 (Figure 7b). Coarse and saddle burial-stage calcian dolomite precipitates from brines flushing internodular zones in the basal anhydrite. After the initial precipitation of limpid dolomites in the primary-textured halite intervals, dolomite crystals continue to grow and re-equilibrate into higher temperature forms (driven by ongoing burial). This is shown by the evolving carbon and oxygen isotope signatures, as well as $^{87}Sr/^{86}Sr$ ratios, which all define a burial trend from early limpid dolomite through coarsely crystalline dolomite through to saddle dolomite with precipitation signatures indicating increasingly higher temperature basinal fluids (Figure 7a; El Tabakh et al., 2003; Warren, 2000). Likewise, $^{87}Sr/^{86}Sr$ ratios define a burial trend from early limpid dolomite through coarsely crystalline dolomite through to saddle dolomite indicative of increasing interaction with basinal fluids (Figure 7b; El Tabakh et al. 2003).

As basal anhydrite is a fractionated dissolution breccia, which is accreting nodules on its upper side and dissolving from the underside, mesogenetic dolomite crystals continue to grow and re-equilibrate into higher temperature forms in the basal anhydrite in response to the same ongoing flushing of rising burial fluids across regional fluid flows focused along the underside of the dissolving salt mass.

In most burial situations, a basinal aquifer carrying hot brines facilitates re-equilibration of the earlier dolomite rhombs into coarse and saddle dolomites. In the case of the basal anhydrite unit, the evaporite unit has yet to be wholly dissolved and re-

Basin	Age	Reference
Levant Basin	Messinian	Meilijson et al., 2018
Granada Basin	Tortonian	López-Quirós et al., 2018
South Pyrenean foredeep	Eocene	Rosell and Orti, 1980
Savannakhet Basin	Cretaceous	Ren et al., 2018
Zechstein Basin	Permian	Humphrey et al., 2019
Delaware Basin	Permian	Presley, 1987
Maritimes Basin	Carboniferous	Lynch and Giles, 1996
Elk Point Basin	Devonian	Williams, 1984
Canning Basin	Devonian	Cathro et al., 1992
Precaspian Basin	Silurian	Okere and Toothill, 2012
East Siberian Basin	Cambrian	Aitken, 1981
Mackenzie Basin	Early Palaeozoic	Aitken, 1981

Table 1. Various basins with possible dissolution-derived basal anhydrites (in part after Warren, 2016).

mains as a fractionated dissolution reside. The halite has gone, but the anhydrite remains and continues to evolve into sparry $CaSO_4$ crystals. An overprint of the early limpid rhombs by later diagenetic neomorphism has yet to occur. Hence it is a unique window in the realm of dolomite diagenesis in an interval not complicatednce of earlier platform carbonates. Burial dolomites are clearly evident here with burial distinctive isotope plotfields because the anhydrite matrix in which they grow appears is a burial-diagenetic unit that has formed in the mesogenetic realm over the vast region on the reactive underside of halite across Khorat Plateau of Southeast Asia. Saddle dolomite is not present in the overlying halite (impervious) and only present in the uppermost part of the underlying sandstone. This is perhaps one of the few undeniable examples of saddle dolomite formed as a primary burial precipitate (not a replacement of an earlier form of dolomite)

The laminar underside of the basal anhydrite is made up of what remains after the anhydrite is dissolved, namely, an undulose cm-thick microlaminar organic-rich insoluble residue layer containing patches or zones of non-planar dolomite crystal aggregations. It also contains calcite micronodules and fissure fills of metal sulphides (mostly pyrite and bornite) created by metal fixing and driven by thermochemical sulphate reduction (Warren 2000).

Overall this "upside-down" anhydrite cap rock is very similar to a pressure solution mega-seam in the metamorphic realm with saddle dolomite forming in the mega-seam. Likewise, its diagenetic mode of formation is not all that dissimilar to a mega-stylolite, except that the fluid flow is more one-sided. This salt-dissolution fractionation model, explaining laterally extensive, constant thickness basal anhydrites with characteristic saddle dolomite crystals on the undersides of thick halites as a form of dissolution residue, has implications for other evaporite basins that possess basal anhydrite units with near-constant thickness (Table 1).

Sparry anhydrite, sparry calcite, saddle dolomite and TSR

Anhydrite is the dominant source of the reactive sulphate in many documented examples of active thermochemical sulphate reduction (TSR) in gas fields worldwide (e.g., Krouse et al., 1988; Worden and Smalley, 1996; Heydari, 1997; Cai et al., 2003, 2004; Zhu et al., 2015). Such anhydrite is generally found in close proximity to newly-minted saddle dolomite and coarse calcite burial spar. These are typical associated carbonate and recrystallised evaporite textural indicators of TSR being active in the deeper burial realms, along with variably present pyrobitumens. The carbonates show isotopic signatures indicative of

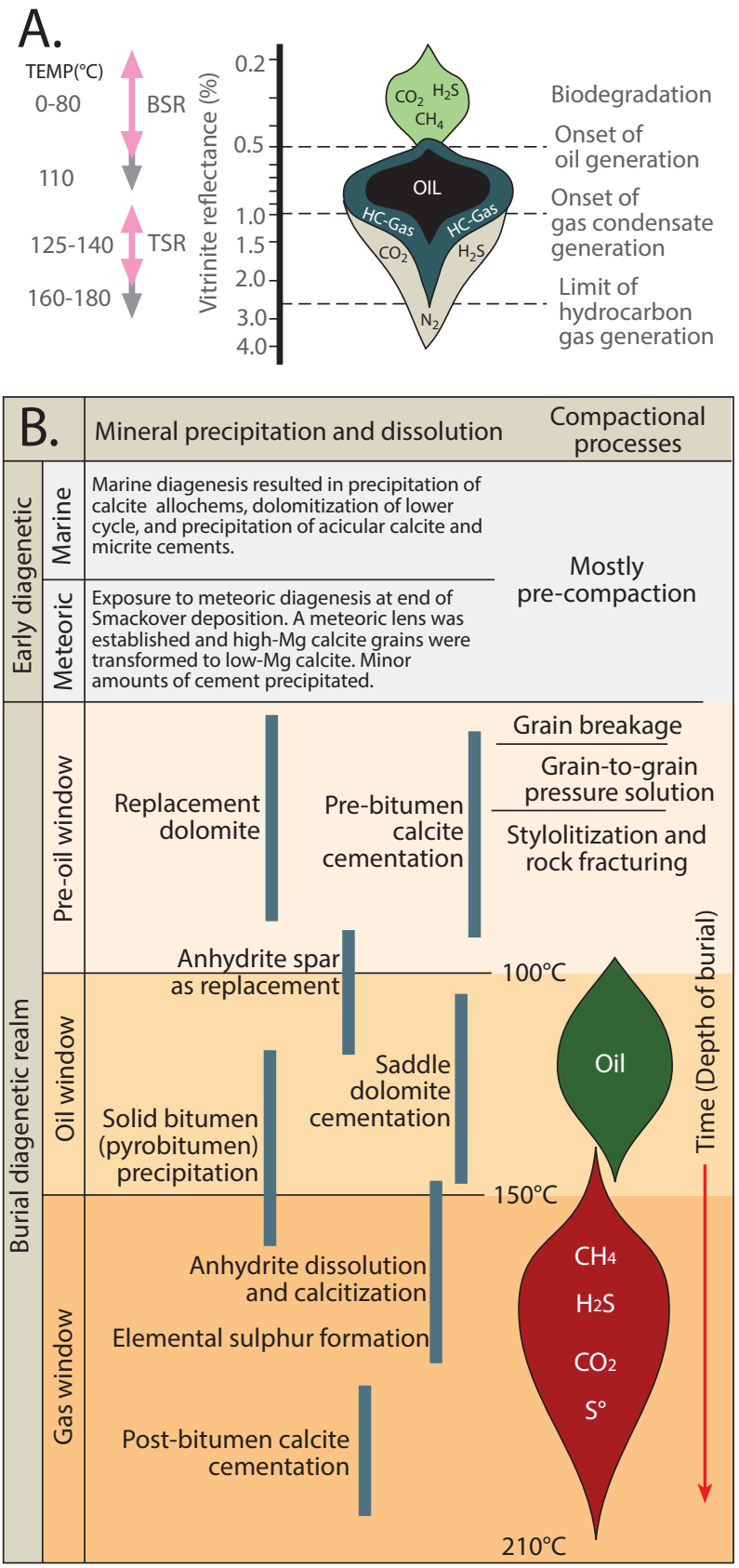

Figure 8. Thermochemical sulphate reduction. A) Thermal regime and hydrocarbon generation stages tied to characteristic values of vitrinite reflectance (after Warren, 2016. B) TSR within paragenetic sequence of the Smackover Formation at Black Creek Field summarizing major products of marine, meteoric, pre-oil window, oil window, and gas window diagenetic stages (after Heydari, 1997).

Occurrence and age of host	Burial anhydrite fabric and subsurface temperature at time of precipitation	Burial calcite spar and saddle dolomite styles	Reference
Yacoraite Fm. (Upper Cretaceous), Argentina.	Sparry anhydrite cement, containing hydrocarbon inclusions and brine, fills intergranular, mouldic and vuggy porosity in a carbonate host. Indicates anhydrite precipitated at 121-137°C from 17% equiv. wt. NaCl brine (NaCl-$MgCl_2$-Na_2SO_4-NaH-CO_3-$NaCO_3$ basinal brine).	Intergranular, mouldic and vuggy primary porosity was reduced by quartz overgrowths, anhydrite cement and bitumen, and was increased by dolomite recrystallization in burial and fracturing.	Cesaretti, 2000
Maha Sarakham Fm. (Upper Cretaceous), NE Thailand.	Coarsely crystalline saddle dolomite rhombs float within a matrix of coarse, recrystallized anhydrite spar in the Basal Anhydrite. Isotopes indicate dolomite precipitated at temperatures ≈ 72-123°C.	Saddle dolomite growth within the recrystallising burial anhydrites of the basal anhydrite	El Tabakh et al., 2003; This article
Smackover Fm. sandstones,Mississippi Basin (Upper Jurassic), Gulf of Mexico.	Anhydrite both as poikilotopic spar masses in which detrital grains are replaced and as smaller patches that have replaced single detrital grains. Precipitation temperatures >100°C. Anhydrite is a relatively late cement and postdates all other volumetrically significant authigenic phases in the sandstones, including K-feldspar, dolomite, quartz, and most calcite cements.	The dolomite is present as small clear rhombic crystals e, frequently encased by the quartz overgrowths, indicating that limpid dolomite preceded quartz cementation. Anhydrite is never observed to inhibit the formation of quartz overgrowths and, as in the Louisiana basin, it overlaps and covers quartz overgrowths These relationships suggest that anhydrite is the last volumetrically significant cement to have formed in the Mississippi basin prior to and during TSR.	Dworkin and Land, 1994 Llinas. 2002
Smackover Fm. dolomites, (Upper Jurassic), Gulf of Mexico.	Anhydrite spar partially replaced allochems and prebitumen calcite cements in mesogenetic pores. Solid bitumen precipitated where hydrocarbons were present. Emplaced in temperature range 100-150°C.	Saddle dolomite in Vocation Field is commonly associated with hydrocarbon emplacement and sparry anhydrites, implyinglate diagenetic formation by sulfate reduction processes	Heydari, 1997, 2000 Llinas. 2002
Khuff Fm. (Upper Permian-Lower Triassic), Abu Dhabi, UAE and Saudi Arabia.	In reservoirs hotter than 140°C, anhydrite has been partially replaced by calcite, and hydrocarbon gases have been partially or fully replaced by H2S. This shows that anhydrite and hydrocarbons have reacted together to produce calcite and H_2S	Burial stage poikilotopic anhydrite crystals fill pore spaces between the detrital carbonate components. Crystals are typically 500 mm in length but locally may reach up to 3 mm. Nucleation of calcite during thermochemical sulfate reduction has occurred via topotaxial nucleation on dolomite matrix crystals.	Worden et al., 1996, 2000; Ehrenberg et al., 2007 Al Eid and Al Tawil, 2009
Kurrachine Dolomite, Triassic, Syria	Following fracturing and mesogenetic leaching by sulphate-bearing warm fluids, significant vuggy porosity was created, but was subsequently occluded by anhydrite burial cements made up of coarse mosaic anhydrite spar and occasional poikilotopic spar.	Saddle dolomite rhombs are patchily scattered through the replacement dolomite host and also occur in veins. In some cases formation of vein-filling crystals before chemical compaction is evident. Dolomite dissolution and anhydrite precipitation took place in the deep burial diagenetic realm following dolomite formation (mostly via brine reflux) and chemical compaction	Hips and Árgyelán, 2007
Prider Fm. (Lower Permian) Kansas, USA.	Burial stage poikilotopic anhydrite cement replaces echinoderm fragments, parts of oncolites, some dolomite spar, and some stylolite seams. Anhhydrite spar recipitation occurred in the range 65-90°C, with a few samples possibly up to 150°C.	During the Late Permian, reflux of low-temperature (≈50°C), Mg-bearing brines precipitated U-bearing dolomite and replaced earlier dolomite in the lower Krider Member and other members of the Chase Group. These brines were most likely associated with the regional deposition of ovwerlying Sumner or Nippewalla Group evaporites.	Luczaj and Goldstein, 2000
Rotliegende Fm. (Lower Permian), onshore and offshore NW Europe.	Poikilotopic sparry anhydrite enclosing sand grains. Distribution shows a strong fault/fracture control to sparry anhydrite in sandstones. Precipitation temperatures in the range 120-140°C.	Micro- and fine-crystalline dolomite formed early in the depositional history and was leached before compaction to form vuggy porosity in the upper two reservoir units and especially at the top of the oolitic grainstone facies.	Duguid and Underhill, 2010; Gauthier et al., 2000; Sullivan et al., 1994
Swan Hills Fm. (Middle to Upper Devonian), Canada.	Coarse bladed crystals of sparry anhydrite enclosing dolomite clasts and possibly related to faults. Fluid inclusions in the anhydrite show crystals formed from basinal fluids at temperatures in excess of 90°C. Machel (2013) documents the wider occurrence of burial anhydrite in Devonian carbonates in the Alberta Basin, than previously noted.	The bulk of the secondary anhydrites appear to have formed as by-products of pervasive dolomitization, which is indicated by the common association of dolomite and anhydrite and the common absence of anhydrite in limestones. Hence, the fluid that formed the bulk of the replacive anhydrites most probably is the same fluid that formed the bulk of the pervasive dolomites.	Krouse et al., 1988; Duggan et al., 2001; Machel, 2013
Dirk Hartog Group, (Silurian) Gascoyne Basin, Australia.	Sparry anhydrite includes blocky poikilotopic cement filling interparticle and mouldic pore spaces in oolitic horizons, and as a bladed cement in larger, often vuggy pore spaces. Formed at elevated subsurface temperatures.	Coarse void-filling dolomite is volumetrically important and forms medium to very coarse crystals that range from 40 to 150 µm. These dolomites are found as clear void fillings and replacing earlier cements in voids between grains. They predate sparry anhydrite cement.	El Tabakh, et al., 2004
St Peter Sandstone (Ordovician) Michigan Basin, USA.	Late stage sparry anhydrite cements that precipitated in crosscutting fractures and postdates with late stage dolomite that had also precipitated at higher burial temperatures	The St. Peter Sandstone was an important migration pathway for many different types of fluids in the Michigan Basin, and the proposed fluid origins indicate that both upward and downward cross-formational fluid flow occurred during the Paleozoic. Older and younger modified seawater produced most of the burial dolomite in the St. Peter Sandstone	Winter et al., 1995
Sinian (Precambrian) dolomite reservoirs in the Sichuan Basin, China	The sulphur isotope compositions (δ34S) of gypsum, H2S, and secondary pyrite sampled from the Sinian Dengying Formation showed that H2S was generated by a moderate thermochemical sulfate reduction (TSR) during the Jurassic–Early Cretaceous periods..	The sulfur isotope compositions ($\delta^{34}S$) of $CaSO_4$, H_2S, and secondary pyrite sampled from the Sinian Dengying Formation showed that H_2S was generated by a moderate thermochemical sulfate reduction during the Jurassic–Early Cretaceous periods. TSR was terminated by the depletion of SO_4 in the formation water, resulting in a modest H_2S content of 5–10% in the natural gases	Zhu et al., 2015

Table 2. Selected examples of sparry burial anhydrite, it can be associated with or post-date coarsely crystalline and saddle dolomites

warmer basinal parent fluids (Figure 8; Table 2) that are are too hot for bacterial sulphate reduction (BSR). Combinations of two or more such indicators can be intimately intergrown, sometimes within single host crystals of anhydrite or dolomite.

In most cases of TSR in an evaporite interval, the source of the necessary sulphate is anhydrite either as crystalline laths in nodules or as spar. In non-evaporite basins, baryte and not anhydrite, can be the sulphate source for the hydrothermal TSR reactions (Zhang et al., 2019). During thermochemical sulphate reduction, H_2S is produced from sulphate ions, typically from dissolved anhydrite, and is reduced to sulphide at temperatures usually over 140°C, via inorganic reactions with hydrocarbons or other forms of organics. These subsurface temperatures are too hot for any known subsurface microbial life, leftover from bacterial sulphate reduction, to survive (Figure 8a; Warren 2016, Chapter 9).

Reactive hydrocarbons caught up in the TSR reaction are mostly branched and n-alkanes, with lesser cyclic and mono-aromatic species in the gasoline range. Historically, the efficiency of thermochemical sulphate reduction in producing H_2S was inferred from laboratory evidence or elevated levels of sour gas (H_2S-entrained) in deep oil and gas wells, rather than direct observation of subsurface processes (Trudinger et al., 1985; North, 1990). In the past two decades, this has changed, with the direct documentation of TSR-produced H_2S (sour gas) in natural gas reservoirs in the Permian Khuff Formation of Abu Dhabi (Worden et al.,1996; Worden et al., 2000), Permian Zechstein carbonates of Germany (Biehl et al., 2016), Jurassic Arab cycles of Abu Dhabi (Morad et al., 2019) and the Sichuan Basin of China (Hao et al., 2015) along with identification of oil markers that, in association with sulphur isotopes ($\delta^{34}S$), can identify oils that have experienced TSR (Amrani et al., 2012).

Carbon and elemental sulphur isotope data from the gases and minerals in the Khuff Fm. show that the dominant general reaction series starts with the replacement of anhydrite by calcite spar (Worden et al., 2000; Worden and Smalley, 1996; Heydari, 1997):

$$CaSO_4 + CH_4 \rightarrow CaCO_3 + H_2S + H_2O$$

AT the same time, gas chemistry and isotope data also show that C_{2+} gases react preferentially with anhydrite via reactions like:

$$2CaSO_4 + C_2H_6 \rightarrow 2CaCO_3 + H_2S + S^o + 2H_2O$$

Sulphur is generated by this reaction and is locally present, but is also consumed by the reaction:

$$4S^o + CH_4 + 2H_2O \rightarrow CO_2 + 4H_2S$$

The frequently quoted and experimentally observed reaction between anhydrite and H_2S with CO_2 to produce calcite and sulphur:

$$CaSO_4 + 3H_2S + CO_2 \rightarrow CaCO_3 + 4S + 3H_2O$$

has been shown, by gas chemistry, calcite $\delta^{13}C$ and sulphur $\delta^{34}S$ data, to be relatively minor in TSR in the Khuff Formation.

Instead, a direct reaction between hydrocarbons and anhydrite occurs in solution. It takes place within residual pore waters that are initially dominated by carbonate dissolved out of the marine carbonate matrix. The first-formed replacive calcite thus contains carbon that was derived principally from a marine dolomite matrix with a $\delta^{13}C$ signature of 0 to +4 ‰. Continuing reaction leads to the progressive domination of pores water derived by TSR carbonate/sulphate reaction, with a minimum $\delta^{13}C$ of about -30‰ (Figure 9a). The spread of carbon isotope values in the

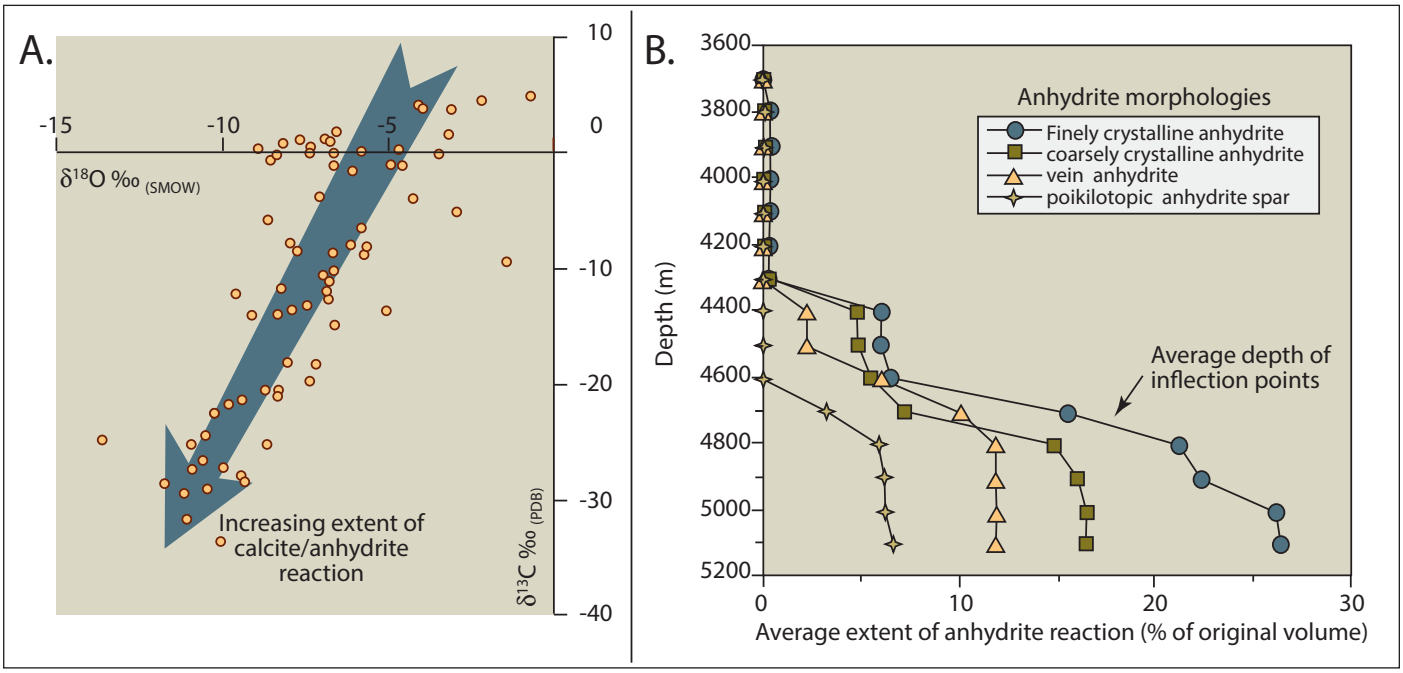

Figure 9. Thermochemical sulphate reduction in the Permian Khuff Fm., UAE. A) Stable isotopes of thermochemical calcite. Arrow shows trend of increasing calcite reaction. B) Depth versus the average extent of anhydrite replacement by calcite for the different types of anhydrite. Anhydrites with smaller crystal sizes are more reactive at any given burial depth. (after Worden et al., 2000).

replacive TSR calcite shows that in the earliest stages of TSR spar the ambient formation water is dominated by bicarbonate derived from dissolution of the matrix and saddle dolomite. As TSR commences, first-formed aqueous carbonate species plus the newly dissolved calcium from the dissolving anhydrite leads to supersaturation with respect to calcite. This calcite is initially inherited the earlier marine-fed dolomite's heavier carbon isotope signature. As TSR proceeded, the methane-derived carbonate come to dominate, leading to ever more negative $\delta^{13}C$ and $\delta^{18}O$ values in the resulting calcite burial spar (Figure 9a).

When petrographically determined amounts of replacive calcite in the Khuff Formation are plotted as a function of depth (Figure 9b) it shows that TSR starts around 4300 m depth (corresponding to a present-day temperature of 140°C) for all of the anhydrite types apart from the coarsest (poikilotopic variety), which shows signs of reaction only below 4,500 m. This implies that availability of sulphate from anhydrite is the rate-limiting step during the earlier stages of reaction when anhydrite is replaced *in situ* by calcite on the very edges of more finely crystalline anhydrite nodules and crystals (Worden et al., 2000).

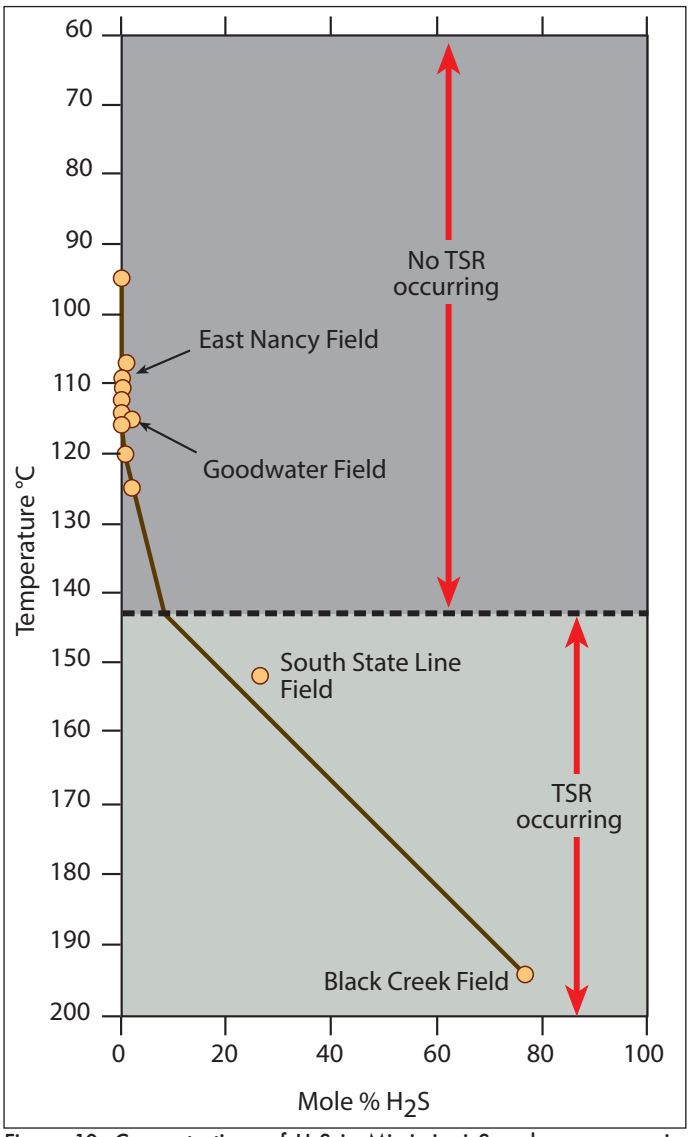

Figure 10. Concentrations of H_2S in Mississippi Smackover reservoirs vary consistently with temperature (after Heydari, 1997)

Worldwide, the lowest temperature at which TSR occurs may be lower than the 140°C seen in the Khuff Fm. Machel (1998) suggests that the onset of TSR occurs in a range from 100-145°C depending on variations in chemical kinetics, which will differ from basin to basin. If so, then one can expect TSR-derived H_2S to form at shallower depths than the 4000 m suggested by the work of Worden et al. (1995) or Heydari (1997).

Thermochemical sulphate reduction produces substantial volumes of very low salinity subsurface water in the vicinity of the reaction zone. Locally, the salinity of formation water in evaporite lithologies undergoing TSR is, therefore, not necessarily high. In the Khuff reservoir the water salinity and isotope data show that the original formation water was locally diluted between four and five times by water from TSR (Worden et al., 1996). A typical Khuff gas reservoir rock volume calculation suggests that initial formation water volumes can only be increased by about three times as a result of TSR. The extreme local dilution shown by the water salinity and $\delta^{18}O$ data in the Khuff must, therefore, reflect transiently imperfect mixing between TSR water and original formation water. Dissipation of this water into surrounding lithologies may aid further dissolution of adjacent evaporites. TSR is believed to cause the dilution of formation waters by up to 50% locally and up to 30% on a reservoir scale (Worden et al., 1996; Yang et al., 2001; Jiang et al. 2013, 2014). On the other hand, there might be other reactions involved in TSR, some of them consuming water, so that the amount of water produced is probably highly variable and, according to Machel (2001), negligible at a regional scale.

Anhydrite dissolution and calcitisation in the Jurassic Smackover Formation in Mississippi, USA, does not occur below temperatures of 140–150°C, suggesting that, as in the Khuff, it is a thermochemical burial process (Figure 8b). Thus, gas window diagenesis in deeply buried dolomitised Smackover reservoirs is largely driven by thermochemical sulphate reduction. Reaction of sulphate with H_2S generates S° that, in turn, reacts with CH_4 to form more H_2S in a self-reinforcing cycle (Heydari, 1997, 2010). Closed-system diagenesis prevents the escape of H_2S and, with sulphate abundantly available (Buckner Anhydrite) but without Fe^{2+} to remove H_2S by pyrite precipitation, the reaction tends to continue until all hydrocarbons are consumed. TSR-generated CO_2 results in precipitation of post-bitumen calcite with negative $\delta^{13}C$ compositions.

Concentration of H_2S in Mississippi Smackover reservoirs varies consistently with temperature (Figure10; Heydari, 1997, 2010). Reservoirs studied are of the same age (150 Ma), similar lithology (clean oolitic limestone), and bounded by impermeable layers (Buckner anhydrite above and lime mudstones below). Heydari (1997) found that concentration of H_2S is very low in reservoirs that have experienced temperatures of 120°C or less for more than 50 m.y. This suggests TSR has not yet occurred, and therefore it is not a time-dependent process and not necessarily kinetically or rate driven. High H_2S concentrations occur in reservoirs with temperatures in excess of 140°C and levels tend to increase with temperature, so suggesting TSR is occurring and is ongoing.

Amrani et al. (2012) defined a set of organo-geochemical criteria for produced oils, which can be used to define the degree of TSR alteration of Smackover oils. Oils that experience TSR exhibit significant ^{34}S enrichment in the [1]benzothiophenes (BTs) compared to dibenzothiophenes (DBTs), while in unaltered oils both compounds have similar isotopic compositions. The $\delta^{34}S$ values of BTs are close to those of sulphate-bearing evaporites of the Smackover Fm., whereas the $\delta^{34}S$ values of DBTs are spread over a wider range and gradually approach those of the BTs (Table 3, Figure 11). They propose that BTs can be a sensitive tracer for the intensity of TSR alteration of an oil or condensate as they form readily under TSR conditions, with large ^{34}S enrichments relative to the bulk oil. In contrast, DBTs exhibit relatively small changes in $\delta^{34}S$, preserving their original $\delta^{34}S$ values longer than do BTs because of their greater thermal stability and slow rate of formation. If this relationship holds in other oil basins then a comparison of the $\delta^{34}S$ values of BT and DBT can be used to detect TSR alteration from the very early stages up to highly-altered oils (Table 3; Figure 11).

Field	Depth (m)	Temp °C	ɾ° (API‰)	H_2S Mole %	S wt%	$\delta^{34}S_{(oil)}$ ‰	$\delta^{13}C_{(oil)}$ ‰	DBT[i] ppm	Thiadiam[ii] ppm
TSR unaltered									
Turkey Creek	4056–4062	93	0.757 (55.5)	0.0	0.8	-0.9	-23.93	431	21
Wallers Creek	4758–4762	126	0.835 (38.0)	0.0	0.1	-12.5	-23.94	192	2
Blacksher	5142–5146	138	0.828 (39.4)	0.0	0.1	5.6	-23.90	270	2
Slightly TSR altered									
Hatters Pond	6005–6011	160	0.756 (55.6)	0.6	0.1	5.1	-23.00	81	20
Cold Creek	6049–6058	160	0.757 (55.5)	0.0	0.1	-0.6	-23.70	118	17
TSR altered									
Appleton	4230–4242	137	0.781 (49.7)	2.0	0.35	10.7	-24.30	691	60
Vocation	4588–4591	127	0.775 (51.1)	5.7	0.3	6.4	-22.50	803	58
Huxford	4835–4841	132	0.774 (51.2)	6.1	0.2	5.7	-22.80	983	43
Chatom	5303–5340	138	0.787 (48.3)	16.7	1.0	12.2	-21.7	1564	149
Big Escambia Creek	5043–5067	143	0.828 (39.4)	30.0	1.4	24.0	-20.85	2345	296
South State Line	5683–5719	151	0.863 (32.4)	31.4	0.8	21.0	-20.13	6313	685

[i] DBT content refer to dibenzothiophene and its alkylated groups including methyl-, dimethyl- and trimethyl-dibenzothiophenes.

[ii] Thiadiam content stands for thiadiamondoids including thiaadamantanes (trimethyl- and tetramethyl-thiaadamantanes), thiadiamantanes (thiadiamantane, methyl-, dimethyl- and trimethyl-thiadiamantanes) and thiatriamantanes (thiatriamantane, methyl-, dimethyl- and trimethyl-thiatriamantanes).

Table 3. Bulk geochemical data for oil and condensate samples from oils in the Smackover Formation (after Amrani et al., 2012 and references therein) with the degree of TSR alteration based on the isotope and DBT thiadiamond characteristics, as determined by Amrani et al., 2012)

1 Benzothiophene is an aromatic organic compound with a molecular formula C_8H_6S and an odor similar to naphthalene (mothballs). Dibenzothiophene (DBT) is an organosulphur compound consisting of two benzene rings fused to a central thiophene ring. It is a colourless solid that is chemically somewhat similar to anthracene. Heterocyclic sulfur compounds such as alkyl dibenzothiophenes and alkyl benzothiophenes are major sulphur components in the hydrodesulphurized oil fractions because they are highly recalcitrant to chemical catalysts

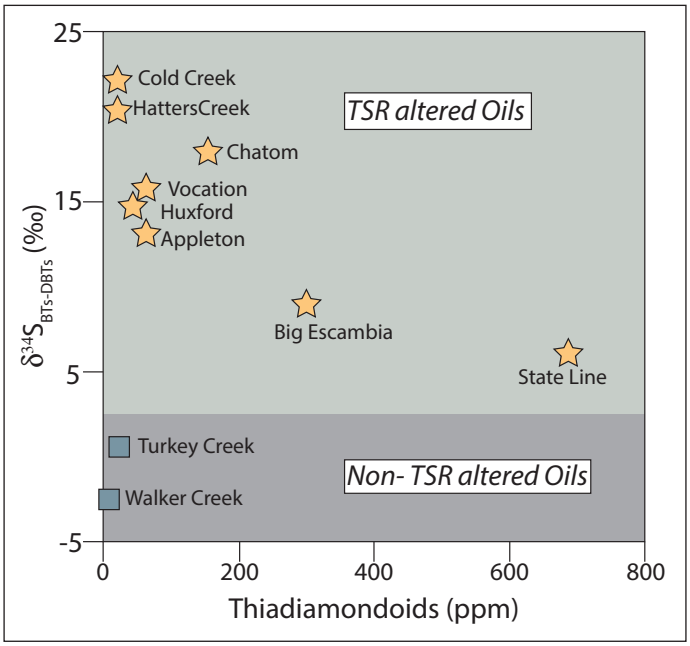

Figure 11. ^{34}S fractionation between BTs and DBTs isomers ($\delta^{34}S$BTs-ΔBTs) as a function of total thiadiamondoid concentration (Table 3), which includes thiaadamantanes (trimethyl- and tetramethyl-thiaadamantanes), thiadiamantanes (thiadiamantane, methyl-, dimethyl- and trimethyl-thiadiamantanes) and thiatri-amantanes (thiatriamantane, methyl-, dimethyl- and trimethyl-thiatriamantanes). The plotted $\delta^{34}S$ values for alkylated BTs and DBTs are the numerical averages of all measured isomers (afer Amrani et al., 2012).

Sour (H_2S-entrained) natural gas, associated with thermochemical sulphate reduction, typifies dolomite reservoirs in the Lower Triassic Feixianguan Formation, Northeast Sichuan Basin, China (Jiang et al., 2014). The sulphate comes from dissolution of the abundant Triassic saltern anhydrites, which also act as seals across oilfields of the region. Reservoirs were initially filled with oil, later replaced by gas during burial to 7,000 m followed by uplift to about 4,000 m. A plot of carbon and oxygen stable isotope clearly breaks out the host matrix limestones and dolomites from the various burial cements. Isotope plots, broken out by timing and texture, defines three separate C-O plot fields, related to pre-TSR, TSR and post TSR calcite cements (Figure 12a). The TSR plot field, with its negative carbon isotope values, overlaps with the TSR plot fields seen in other already discussed examples (e.g. Figure 9).

Pre-TSR diagenesis (in time order), included host neomorphism and recrystallisation of the host dominated by eodiagenetic dolomitization via brine reflux, fracture-related calcite cementation, baryte, quartz, celestite, and fluorite mineralization and a dolomite recrystallization stage at burial temperatures up to 130 °C (Figure 12b). TSR followed, and resulted in anhydrite replacement by TSR-calcite, petroleum destruction, formation of

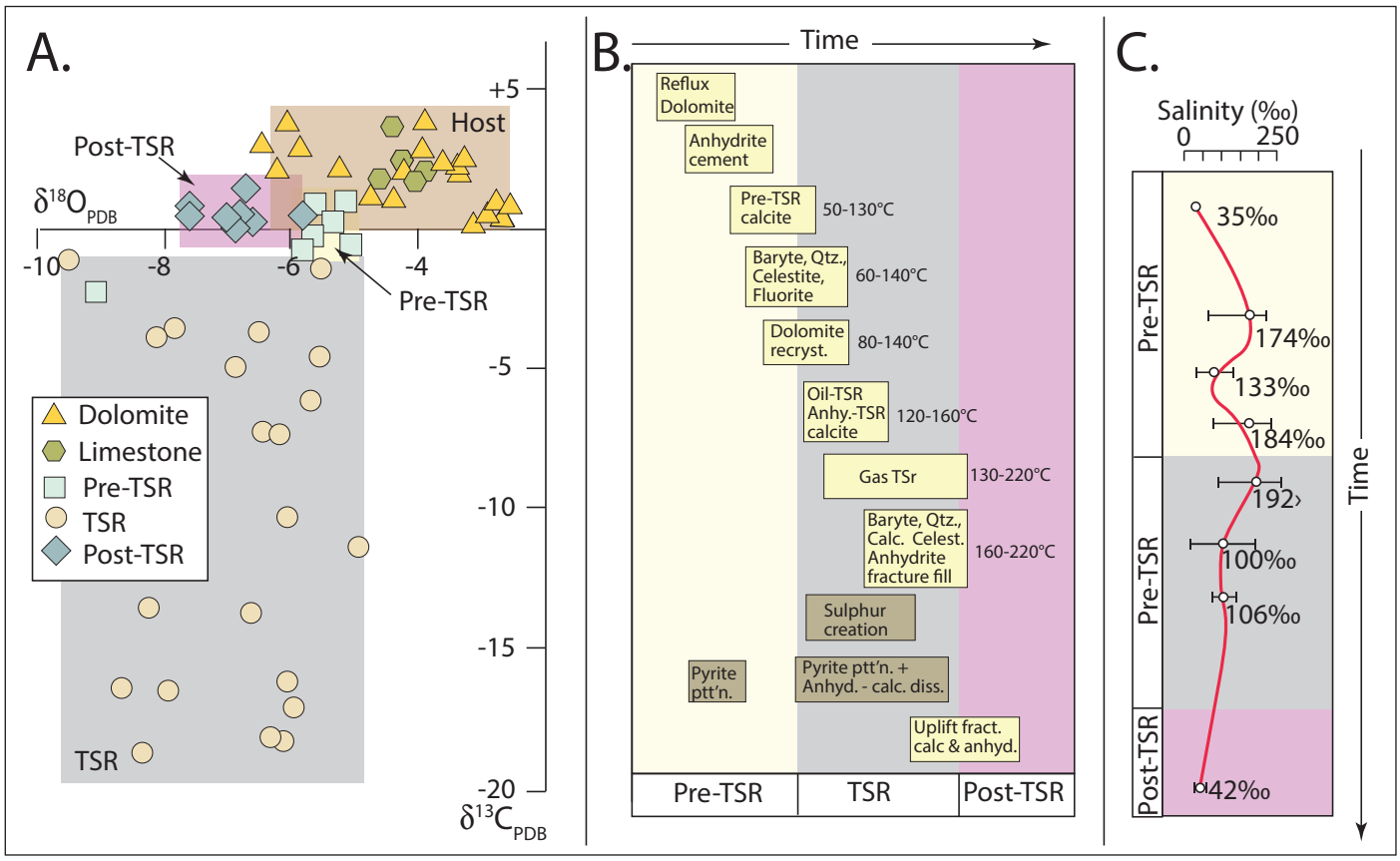

Figure 12. Thermochemical sulphate reduction (TSR) in Jialingjiang Formation, NE Sichuan Basin, China. A) The carbon and oxygen isotopic compositions of Feixianguan Formation host carbonates and the pre, syn and post-TSR isotope fields of the various calcite cements. B) Paragenetic sequence with inclusion-determined temperature ranges, C) Inclusion-determined salinities of the three cementation phases in the calcite cements (after Jiang et al., 2013, 2014, and references therein).

sulphur-rich pyrobitumen and elemental sulphur and generation of large volumes of H_2S, CO_2. Diagenesis during TSR can be subdivided into oil-stage TSR and gas-stage TSR with oil-stage TSR defined by the presence of primary oil and bitumen inclusions in the TSR-calcite.

Based on aqueous inclusion homogenization temperatures, oil-stage-TSR commenced at a temperature of 116ºC with a mode between 130 and 140 ºC (Figure 12b). Gas-stage TSR started at a temperature of 135ºC and continued to maximum burial temperatures of about 220ºC. Trace amounts of pyrite, baryte, quartz and celestite grew during TSR. Post-TSR diagenesis was dominated by fracture-related calcite precipitation as well as celestite and sparry anhydrite crystallization. Formation water salinity increased from depositional values (3.5 wt%) up to 24 wt% during pre-TSR dolomite recrystallization, probably due to an influx of evaporite-dissolution associated water from the overlying Jialingjiang Formation. Later pre-TSR baryte, quartz, celestite, and fluorite mineralization was associated with a transient decrease in water salinity (Figure 12c). During TSR, formation water salinity decreased from 26 wt% to as low as 4 wt%, as a result of fresh water being produced by TSR reactions (Jiang et al., 2014)

The Sichuan example illustrates that, if anhydrite and methane remain in reservoirs reaching 140°C and above, thermochemical sulphate reduction can continue into the low temperature end of the metamorphic realm (>200°C). Alonso-Azcarate et al. (2001) documented vein deposits containing native sulphur, gypsum, quartz and rare sphalerite in the very low-grade greenschist metasediments in Cervera del Rio Alhama of the Mesozoic Cameros Basin, NE Spain. In outcrop the veins are hosted by lacustrine evaporites, which now comprise alternations of dolomite and recrystallised gypsum layers, the latter was anhydrite during metamorphism and converted to gypsum during telogenesis. Fluid inclusion homogenization temperatures and quartz-sulphate oxygen isotope geothermometry indicate formation of the veins around 225° C. Fluid inclusions contain sulphur along with a gas phase comprising H_2S, N_2, CO_2 and minor CH_4. These are all reactants and products of sulphur generation via thermochemical sulphate reduction (TSR) in the anchizone. The conversion utilised organic matter, followed by a partial re-oxidation of some H_2S via SO_4 to then produce sulphur. These TSR reactions differ from those observed in most petroleum-related sour gas settings in that there is no evidence for secondary carbonate precipitation during TSR and in that significant S isotopic fractionation exists between sulphate (around + 20‰) and reduced products (sulphur is around - 11‰).

In all these diagenetic TSR examples there is a reactive connection between the loss of anhydrite and its replacement by poikilotopic calcite spar cement and saddle dolomite, which is often present or forming in the same burial environment. The association between saddle dolomite, the loss of anhydrite and the formation of Pb-Zn ores in Mississippi Valley Type (MVT) deposits is even more evident in the more thermally evolved ex-

Deposit and location	Details	Reference
Deep-burial hydrothermal alteration of the Pre-Salt carbonate reservoirs from northern Campos Basin, offshore Brazi	A paragenesis including saddle dolomite, macrocrystalline calcite, mega-quartz, Sr-barite, celestine, fluorite, dickite, sphalerite, galena, and other metallic sulfides filling fractures and dissolution porosity, and aqueous fluid inclusions with homogenization temperatures of 92–152 °C and salinities between 13 and 26 wt % eq. NaCl characterized a hydrothermal system with some analogy to carbonate-hosted Pb–Zn Mississippi Valley (MVT) and Irish-type deposits. Petroleum inclusions and solid bitumen testify atypical oil generation and migration, associated with the hydrothermal flow	Lima et al., in press
Hydrothermal dolomite reservoir in the Precambrian Dengying Formation of central Sichuan Basin, Southwestern China	Dolomitized reservoir intervals contain planar and saddle dolomite, quartz, solid bitumen and few hydrothermal replacive minerals. Fluid inclusion analyses of dolomite suggests that rocks are formed at temperatures ranging from 132.6°C to 218.7°C in the presence of dense brines, while the dolomite phases are demonstrated by negative δ18O and δ13C VPDB values. Strontium isotopes enriched in 87Sr, and the fluid source could support the conclusion. The dolomites of the Dengying Formation in central Sichuan Basin formed around basement-rooted wrench faults. Widespread solid bitumen in the Dengying Formation reflects the effects of hydrothermal alteration rather than the impact of normal burial-related thermal maturation. Further, the close association of sold bitumen and authigenic kaolinite indicates that natural deasphalting plays a role in the formation of reservoir solid bitumen.	Feng et al., 2017; Gao et al., 2018
Saddle dolomitealteration, and late stage hydrocarbon accumulation in a Middle Triassic carbonate sequence (Szeged Basin, SE Hungary)	Middle Triassic shallow marine carbonates in first stagewere completely dolomitized by reflux of slightly evaporated seawater. Then nonplanar matrix dolomite and saddle dolomite cements formed in the intermediate and/or deep burial realm in the presence of hot (138–235 °C) and moderately saline brines (4.1–8.7 mass% NaCl equivalent) Vuggy, fracture, and solution enhanced porosity are also related to this local hydrothermal invasion. Ccalculated $\delta 18O_{water}$ and the measured $\delta D_{wate}r$ values of the fluid inclusions from the saddle dolomite cement together with the relatively low salinity values indicate a metamorphogenic (and/or magmatic) origin of the hydrothermal fluid that probably was channeled along the Upper Cretaceous subhorizontal overthrust zones. The pores formed by the leaching effect of these hydrothermal fluids were subsequently partly occluded by meteoric calcite during the Paleogene–Middle Miocene subaerial exposur	Garaguly et al., 2018
Fault-controlled hydrothermal dolomites in the MVT deposits of the Riópar area (Prebetic Zone, SE Spain)	Two stratabound dolostone geobodies associated to the W–E trending San Jorge fault and connected by other patchy bodies, Seven different dolomite types incluiding saddle dolomites tied to minerealisation were identified and are isotopically depleted compared to Upper Jurassic to Lower Cretaceous limestone signature along with more radiogenic $^{87}Sr/^{86}Sr$ values for saddle dolomites related to the Zn-(Fe–Pb) sulfide mineralization thatprevailed after fluid interaction with Rb-bearing minerals. Microthermometrical studies on two-phase liquid and vapor fluid inclusion populations in planar and non-planar dolomites and sphalerite show homogenization temperatures between 150 and 250 °C tied to hydrothermal conditions in deep-burial diagenetic environments. \	Navarro-Ciurana et al., 2016
Maoping Pb–Zn deposit, northeastern Yunnan, China	Dolomite in the Carboniferous limestone is part of a spectrum of hydrothermal mineral deposits, and the diagenesis and mineralization processes, in which the acidity of fluids played an important role. Ore-forming fluids had passed throughvugs and fractures, and the locus of massive ore formation was the center of the migrating fluid body. Saddle dolomite was deposited during pauses in sulfide precipitation.	Wei et al., 2015
SFault-focused hydrothermal dolomites in shallow marine carbonates in the western part of the Basque Cantabrian Basin in Northern Spain	Fracture-related hydrothermal dolomites hosted in these Albian carbonates where evealed several dolomite bodies related to main faults curring stratification almost at right angles. Dolomitization is pervasive and independent of the limestone facies. Main dolomite facies are fine replacive, sucrosic and saddle. Polyphase hydrothermal dolomitization occurred at fluid temperatures between 75°C and 240°C in highly variable salinity of up to 22wt.% NaCl. Fine dolomite replaced limestone first and then, sucrosic and saddle dolomites replaced part of the first dolomite and cemented newly created fracture porosity together with different calcite cements. Zebra dolomites and hydroclastic breccias are products of the later stage. Albian stretching of the crust and subsequent ascent of the isotherms in the area is suggested to have produced sufficient heat for the dolomitizing fluids. Fluids moved from subsiding areas to fractured uplifted enhanced by diapiric activity.	López-Horgue et al., 2010
Late diagenetic zebra dolomites in the Middle Cambrian Cathedral Formation: British Columbia, Canada (see Figure 1a)	The late diagenetic zebra dolomites ormed from focalised fluid flow of hot saline fluids (Th maximum = 180–200 °C, Tm,= −18 to −20 °C). $\delta^{18}O$ values vary around − 18.0‰ (VPDB) and $\delta 1^{3}C$ around − 1.35 ‰. 87Sr/86Sr values for the grey (a) replacive dolomite laminae (0.70958 to 0.70970) and for the white, partially replacive laminae and dolomite cement (0.71187 to 0.71228), support involvement of radiogenic fluids which interacted with siliciclastics. Zebra dolomitisation post dates cleavage and is controlled by normal faults. Syn-fracturing dolomitisation in an overpressured regime is invoked for the zebra dolomites formation while the associated coarse crystalline beige dolomites reflect the more passive influx of the dolomitising fluids replacing the host rocks. The fact that MVT mineralisations (Kicking Horse and Monarch deposits), which post-dates zebra formation, occur within a similar structural setting adjacent to the zebra dolomites, suggests that similar fluid flow pathways where re-used several times.	Swennen et al., 2003

Table 4. Selected examples illustrative of the association between saddle and hydrothermal dolomite, pyrobitumen, hydrocarbon reservoirs and Mississippi Valley Type ore deposits (See Warren 2016, Chapter 15 for a more detailed discussion of the literature.

amples of the TSR which are the MVT ores with thermal ranges that pass from the lower end of the diagenetic realms into the lower end of the metamorphic realm

Saddle Dolomite - calcium sulphate - MVT association

Mississippi Valley Type (MVT) Pb-Zn deposits often have saddle dolomite as gangue, as is remnant calcium sulphate, baryte and celestite. Otheres may lack obvious evidence of calcium sulphate or its remnants (Table 2). We shall focus on those with calcium sulphate. One of the best-documented examples comes from the Cadjebut Region on the Lennard Shelf of the Canning Basin, West Australia where there is a documented link between ore deposition, metalliferous chloride brines (from dissolution of halite deeply buried in the Fitzroy Trough and flushing metals as they rise) and commodity fixation at sites of marginward sulphate /organic /hydrocarbon fixation at the fault-defined edge of the Lennard Shelf. Worldwide, many of the larger MVT deposits show an association with evaporites (Figure 13; Warren, 2016, Chapter 15)

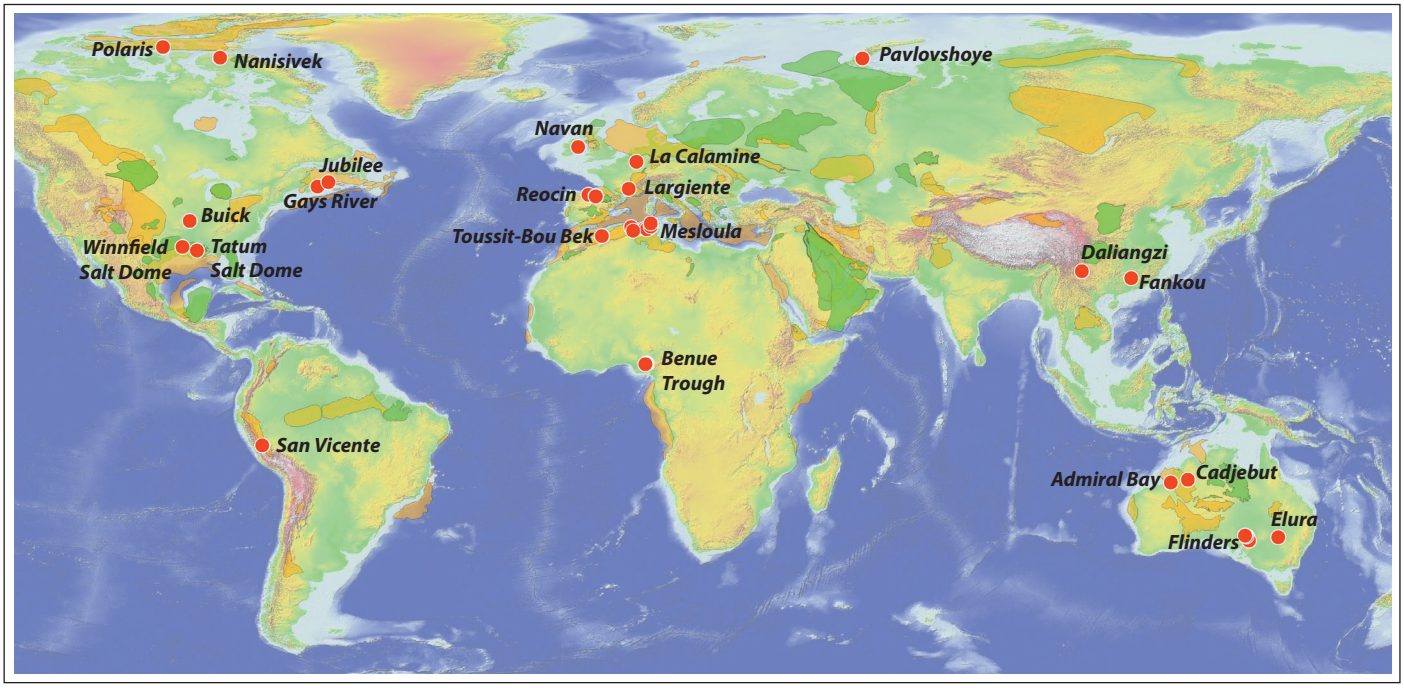

Figure 13. Map showing some of the various MVT ore deposits worldwide with an ore genesis tied to the presences of evaporites and generally found at metal fixation sites where hydrothermal saddle dolomites occur (compiled from the SaltWork database - See Warren 2016, Chapter 15 for a more detailed discussion).

Bedded calcium sulphate evaporites and their lateral dissolutional equivalents define rich MVT ore horizons, and prior to mining, were extensively cored by BHP Minerals in the area around the Cadjebut Mine. The region is an example of hydrothermal karst development in a platform saltern. Variably mineralised evaporite solution breccias (rock matrix breccias) are the lateral equivalents of the Pb-Zn mineralised sequence in the Cadjebut Mine. This MVT deposit undoubtedly represents one of the best-documented examples of *in situ* burial replacement of evaporite beds by Pb-Zn sulphides on a one for one basis (Fig-

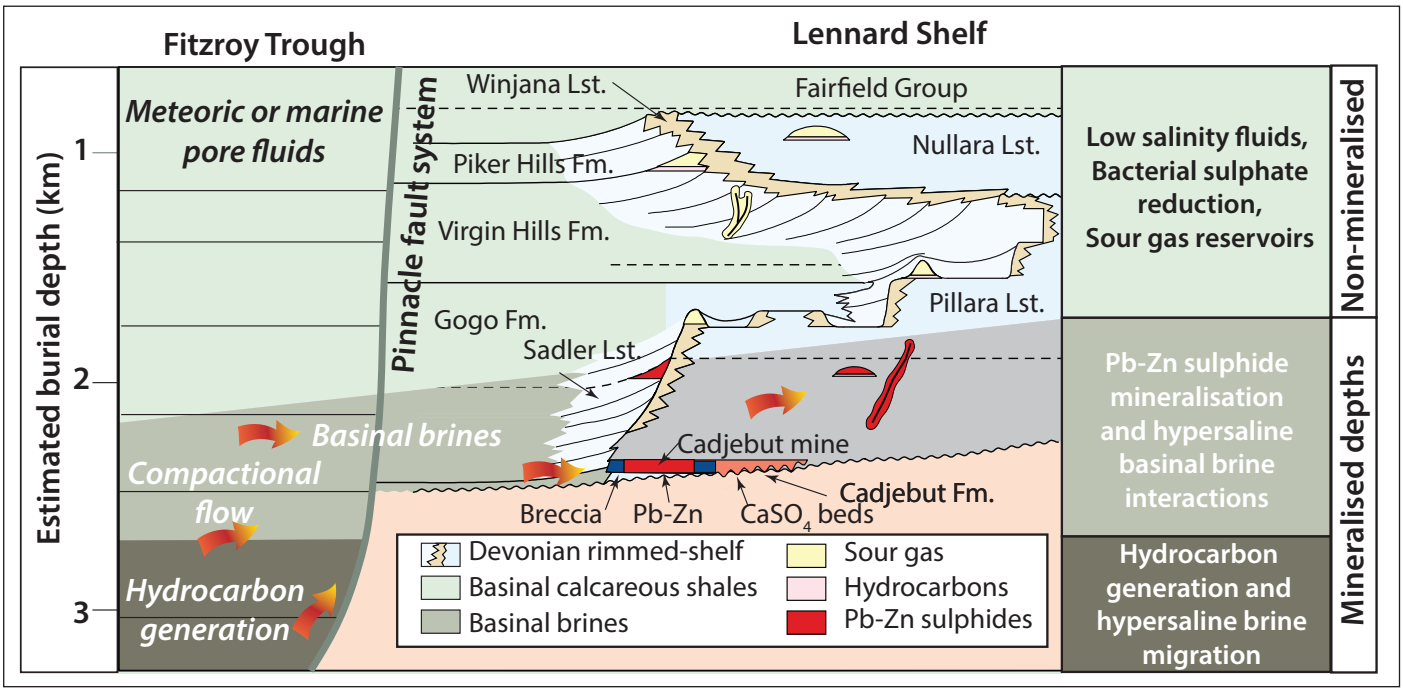

Figure 14. Conceptual model for MVT sulphide precipitation on the eastern Lennard Shelf. At around 350 Ma, sediments of the Fitzroy Trough expelled metalliferous basinal brines and mature hydrocarbons by compactional flow. In shallow subsurface environments with low salinity and low temperature (60–70°C) fluids, bacterial sulphate reduction occurred in and around saltern evaporite seals and hydrocarbon reservoirs within the Devonian platform. Sulphate reduction was largely fed by Givetian saltern $CaSO_4$ evaporites (Cadjebut Formation) and H_2S-rich reservoirs higher in the stratigraphy form in a variety of traps (faults, antiforms, and stratigraphic traps). Sulphides are precipitated when basinal brines interact directly with evaporites or invade intervals of trapped H_2S-rich (modified from Warren and Kempton, 1997; Playford & Wallace,2001; Wallace et al., 2002, Kerans and Harris, 2008).

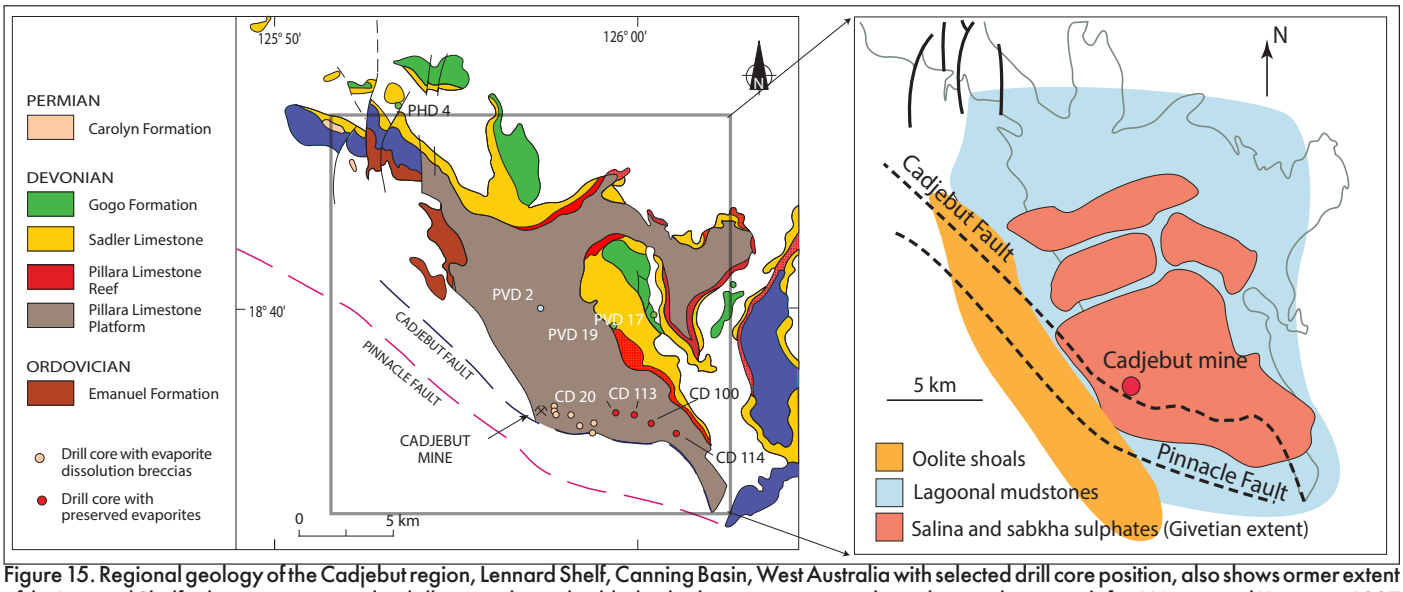

Figure 15. Regional geology of the Cadjebut region, Lennard Shelf, Canning Basin, West Australia with selected drill core position, also shows ormer extent of the Lennard Shelf saltern, as recovered in drillcore, either as bedded anhydrite or evaporite solution breccia horizons (after Warren and Kempton, 1997

ures 14, 15a, b; Tompkins et al., 1994a,b; Warren and Kempton, 1997). That is, the pre-existing evaporitic mudflat beds are directly replaced by Pb-Zn sulphides and dissolving calcium sulphates were the sulphur source to the metal sulphides. The sulphate to sulphide replacement process occurred across cm- to metre- sized cavities, and so the banded and breccia replacement textures are layered, sometimes forming "zebra" textures. This cavity infill replacement process means that not all the ore textures are a direct mimicry of the precursor laminar to nodular evaporite textures, some infill cavernous porosity (Tompkins et al., 1994a versus Warren and Kempton, 1997).

Regionally, the Cadjebut ore deposit is a Mississippi Valley Type (MVT) deposit hosted within the Givetian anhydrite entraining Lower Dolomite unit of the Cadjebut Fm. ramp. This sand-shoal-rimmed ramp was the depositional setting that immediately preceded the reef-rimmed Pillara Limestone platform, which defines the Lennard Shelf (Figure 14). Regionally, the Givetian depositional setting can be divided into two zones: a) a higher energy shoal region in the vicinity of the mine and Cadjebut Fault and, b) a landward more restricted, lower energy, at times evaporitic, lagoonal setting laid down in a series of shoaling carbonate cycles (Figure 15). The upper portion of each cycle is characterized by an evaporitic cap of laminar dolomitic siltstone and mudstone with associated nodular anhydrite that formed a laterally extensive facies mosaic of sabkhas and salinas across an evaporitic mudflat. This originally shallow subaqueous or sabkha mudflat gypsum converted to nodular anhydrite during shallow burial and was subsequently replaced by Pb-Zn sulphides in the mine area (Figure 16)

Three petrographically distinct forms of dolomite occur in the lower dolomite unit across the Cadjebut region (Figure 17): a) a regional finer-grained non ferroan mimetic form with $\delta^{18}O_{PDB}$ of -2 to -4‰ - this dolomite and b) a ferroan medium to coarsely crystalline form with $\delta^{18}O_{PDB}$ -4 to -7‰ that is best developed about major growth faults. This dolomite overprints and replaces the finer-grained stratabound mimetic dolomites as well as other carbonate facies. The finer-grained ferroan dolomite formed by syndepositional brine reflux associated with the deposition

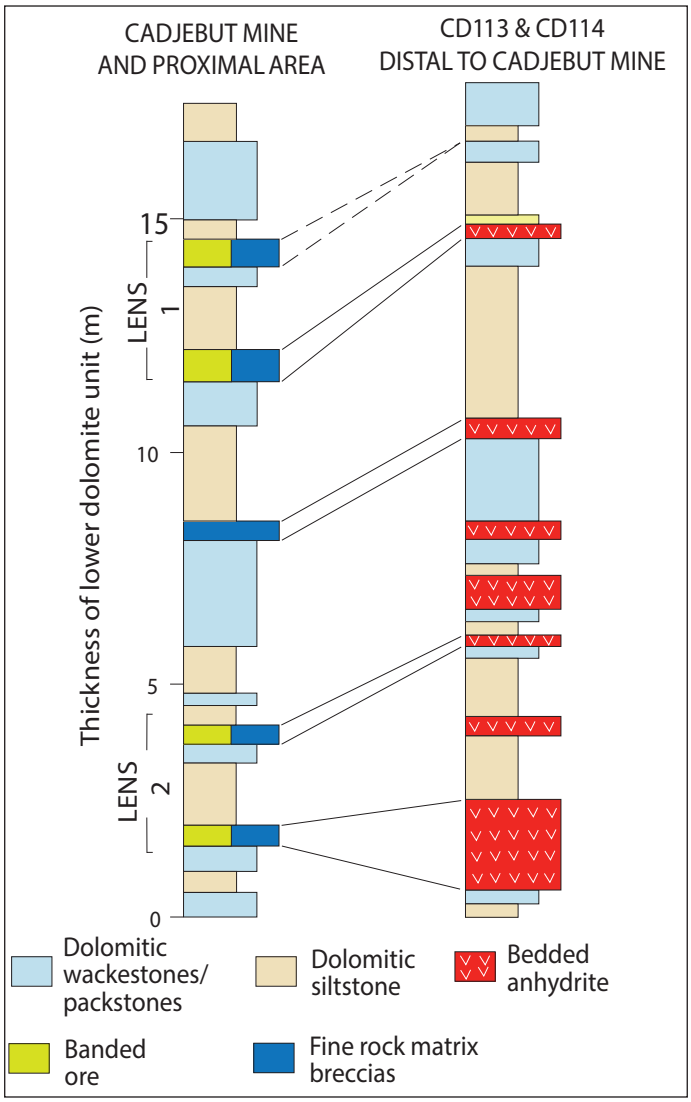

Figure 16. Correlation panel showing lateral equivalence between ore horizones and evaporite bed still present som distance from the mine (see Figure 15a for corehole position).

of evaporites, while the coarser more ferroan dolomite formed during burial from escaping basinal fluids. These same fluids

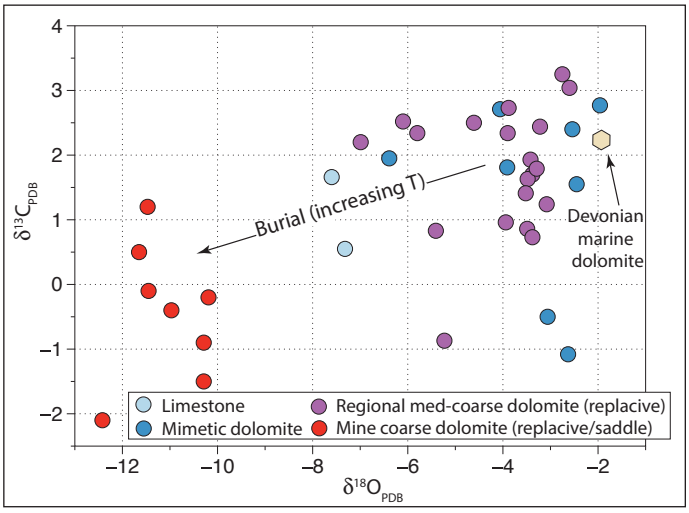

Figure 17. Plot of $\delta^{18}O_{PDB}$ versus $\delta^{13}C_{PDB}$ for various dolomites in the Cadjebut mine and its surrounds (after Warren and Kempton, 1997).

later carried metalliferous fluids from the Fitzroy Trough into sites of ore formation. Post-ore coarse replacement and saddle dolomites from the Cadjebut mine constitute the third dolomite type and are further depleted in $\delta^{18}O_{PDB}$ (-10 to -12‰) and likely indicate localized somewhat elevate thermal conditions related to sulphide mineralization.

Interaction of a metalliferous basinal brine with sulphate that was derived from the dissolving anhydrite beds precipitated the various ore lenses at Cadjebut mine. Sulphide-mineralised horizons in the Cadjebut mine can be correlated on a one to one basis with fine-rock matrix breccia horizons in the immediate area around the mine and with remnant bedded sulphate units well away from the mine (Figure 15a, b).

Two dominant ore types are present (Figure 18a): (a) stratiform, rhythmically banded zinc-rich ore; and (b) stratiform to stratabound, lead-rich breccia-hosted cavity-fill ore. The rhythmically banded ore occurs as four stratiform horizons, two throughout lens 2 and two in the northern part of lens 1. Rhythmically banded baryte and/or rhythmically banded marcasite form a halo around the orebody and are associated with the rhythmically banded zinc-rich ore.

The rate of evaporite dissolution versus the rate of supply of mineralising fluid controlled the large scale textures within the Pb-Zn ores (Warren and Kempton, 1997). Lead-zinc mineralisation in the Cadjebut Mine occurs as three distinct ore types (Figure 18a):

- Stratiform rhythmically-banded zinc-rich ore,
- Stratiform Type A ore-matrix breccia ore, and
- Crosscutting Type B ore matrix breccia ore.

The rhythmically-banded ore formed under conditions where the potential for sulphide precipitation exceeded the rate of evaporite dissolution. This occurred in cm-sized laminar dissolution meshworks that ate their way into the anhydrite beds (Figure 18b). Millimetre-laminated colloform to pendulous microstalactitic sphalerites were the dominant precipitates. Type A ore matrix breccia formed in irregular cm-dm stratabound cavities. These formed at times when the rate of sulphide precipitation was slower than the rate of sulphate dissolution. Such hypo-

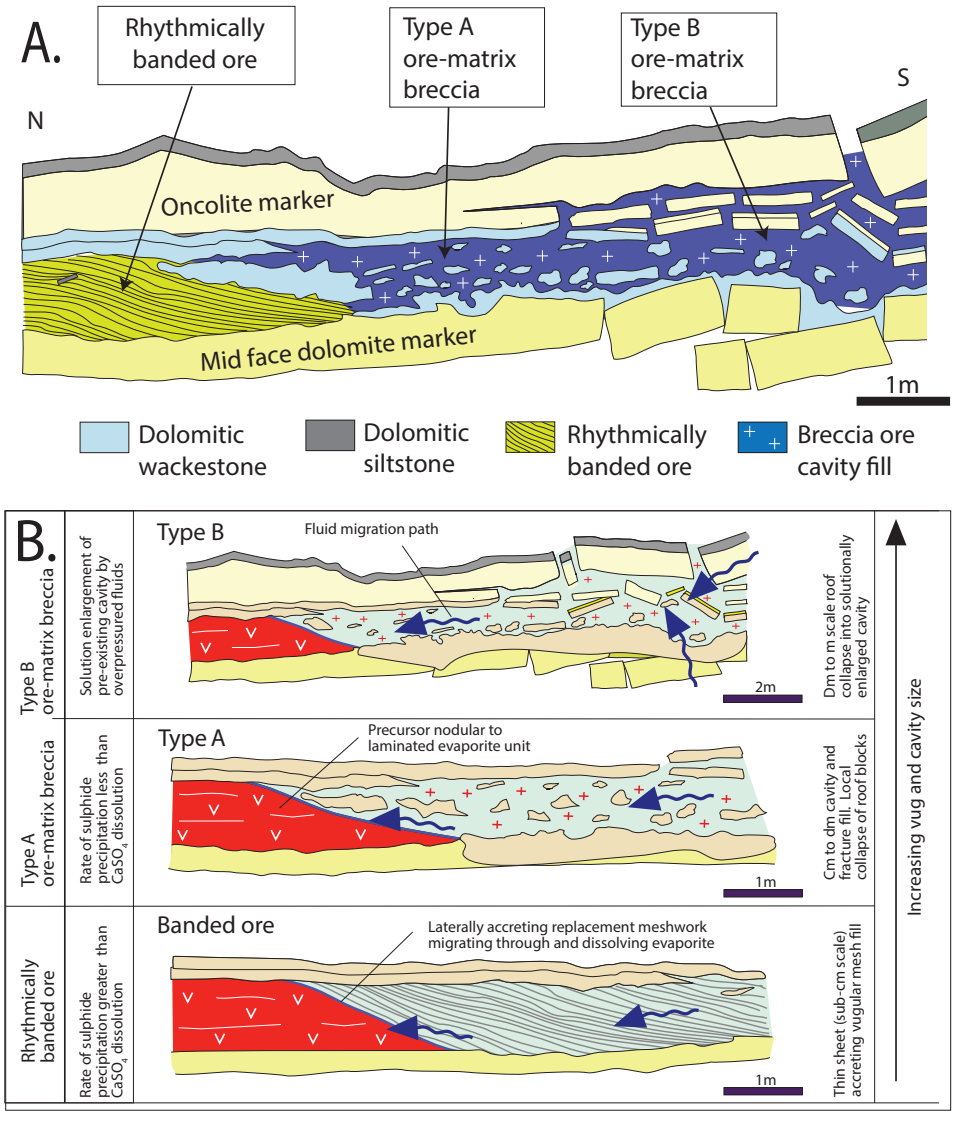

Figure 18. Ore Textures in Cadjebut Mine. A. Nature of mineralisation (type A and B)in intervals of evaporite solution collapse brecciation, as mapped in mine panels in the former Cadjebut Mine. B) Schematic showing controls on ore texture reflect an interplay between rate of supply of metalliferous fluid and the rate of evaporite dissolution (after Warren and Kempton, 1997).

gene cavities were not sufficiently large to instigate catastrophic roof collapse. Type B ore-matrix breccia ores formed in dm-metre sized cross-cutting cavities, fractures and veins. Cavern space was sufficiently large to allow the single-event roof span collapse and rotation of metre-sized roof blocks into the caverns. Type B ore-matrix breccias are lead-rich compared to the banded ore and are interpreted by Tompkins et al. (1994) to postdate the formation of banded ore.

All the Cadjebut ore textures were created from sulphate supplied by the dissolving evaporites across mm-dm-sized replacement fronts or meshworks under deep bathyphreatic and likely overpressured gassy conditions (Warren and Kempton, 1997).

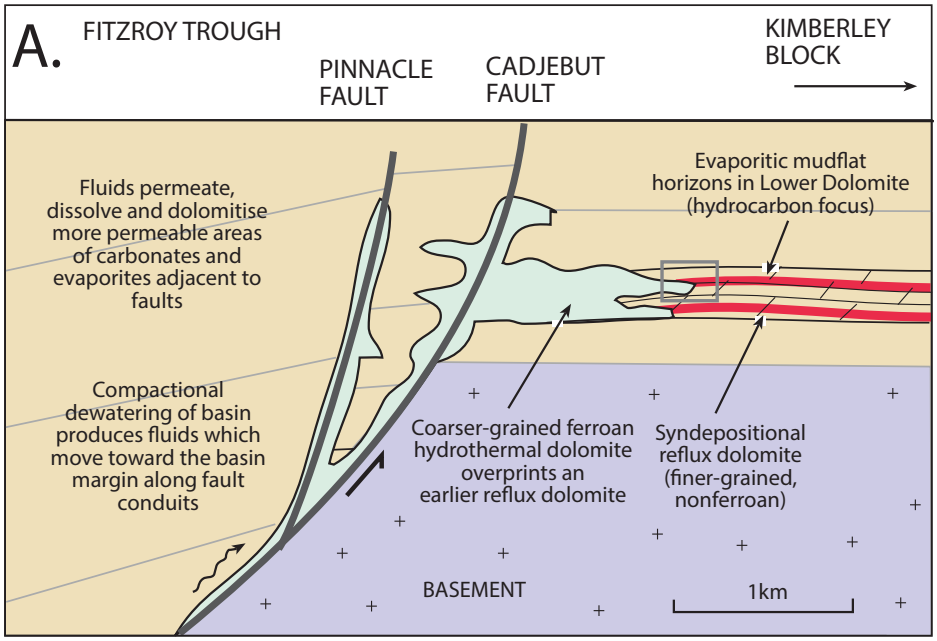

Figure 19. Cadjebut MVT ore, NW Australia. Schematic cross section showing the relationship between basinal fluids moving up along regional extensional faults to act as sources for burial dolomite in the platform carbonates, and the focusing/replacement t effect of sulphate beds in the evaporitic mudflat sediments of the Lower Dolomite (rectangle indicates zone of sulphide mineralisation).

There is a one-to-one correlation of sulphide-mineralised horizons in the Cadjebut Mine with evaporite dissolution breccia horizons in the immediate area around the mine, and with remnant bedded anhydrite units away from the mine (Figure 16). Calcium sulphate beds were the precursor lithology to the sulphide ore lenses at Cadjebut. The stratabound linear nature of the Cadjebut deposit reflects a time when upwelling metalliferous basinal fluids interacted with bedded stratiform nodular anhydrite beds and trapped hydrocarbons to precipitate lead and zinc sulphides.

Current structure in the mine region preserves a gentle drape anticline, which Warren and Kempton (1997) interpret as a partial artefact of the mineralisation structure, enhanced by the sequential loss of the surrounding evaporites, after ore had locally replaced a bedded anhydrite precursor. The linear nature of the anticlinal structure indicates some form focusing of ore fluids and hydrocarbons, either atop an active underlying fault, or within a pre-existing anticlinal trap, perhaps created as a rollover drape on the edge of a evaporite-dissolving front (e.g. Figure 19). Hydrocarbon residues (bitumens) are still present in the ore zones.

The precursor host lithology to the various ore horizons at Cadjebut are massive to bedded nodular anhydrite beds. The stratabound linear nature of the Cadjebut deposit reflects a time when metalliferous basinal fluids encountered bedded stratiform nodular anhydrites causing them to precipitate lead and zinc sulphides. This process locked in place a mineralization event at the stratigraphic position of each evaporite bed in the lower dolomite unit. Conduits for the metalliferous basinal fluids were the basin-margin-defining faults such as the Cadjebut and Pinnacle Faults. Fine-matrix breccias define subsurface evaporite dissolution both prior to and after the sulphide mineralization event. Saddle dolomite formed from basinal fluids at the same time. Today the remnant nodular anhydrite beds are rehydrating to satin-spar and poikilotopic gypsum as modern groundwaters seep into the units.

One of the problems with comparing nodular calcium sulphate and open-space filling zinc and lead sulphide textures in the Cadjebut region occurs when modern telogenetic effects go unrecognised as they do here and in other MVT deposits where $CaSO_4$ remains in the mine area. Much of the shallow anhydrite that was cored in the 1980's and 1990's is converting to porphyroblastic gypsum down to depths of hundreds of metres as it is flushed by modern meteoric waters (telogenetic alteration). Some workers (Tompkins et al., 1994a) did not realise that the current gypsum textures in relict anhydrite beds recovered in cores are replete with such telogenetic rehydration features (tertiary evaporites).

Such gypsum rose and cannonball textures should not be compared to possible primary depositional textures (erroneous assignment to a sabkha for massive sulphate units), nor to cavity fill and layered textures in the metal sulphides that formed in the mesogenetic realm. Ore evolution models that do not remove the effect of modern gypsum overprints, or any assumption that gypsum textures in recovered cored could be primary (has survived kilometres of burial and uplift) are erroneous. Respective precipitative processes for anhydrite rehydration and metal sulphide textures at Cadjebut are totally unrelated in terms of time and space (Warren and Kempton, 1997).

The now depleted Cadjebut Mine deposit is the largest and most concentrated of a number of MVT accumulations in the Lennard Shelf Pb-Zn province, mostly hosted in Devonian shelf carbonates, although the Cadjebut is deposited in ramp dolomites of the Givetian Cadjebut Fm, which immediately underlies the Frasnian- Famennian rimmed-margin dominated by the Willara

and Pillara platforms (Figure 13; Hocking et al., 1996). The rimmed-margin Frasnian-Famennian platform-hosted deposits include hydrothermal-karst dominated deposits (Goongewa and Bloodwood), and fault or fracture-hosted deposits (e.g. Pillara (aka Blendevale), Kapok, Fossil Downs). Fault and fracture-hosted mineralization style dominates Frasnian and Famennian platform host across the Lennard Shelf (Wallace et al., 2002).

The Goongewa deposit is situated in the hanging wall of a normal fault (Cadjebut Fault). Stratigraphically, the mineralisation occurs around a Givetian platform margin and also occurs at the boundary between dolomitised and undolomitised carbonates. MVT sulphides there are largely present as cavity-filling cements within large hydrothermal karst caverns. The nearby Kutarta mineralisation (close to the old Price's Creek prospect) has a quite different style again, with much of the base-metal sulphide mineralisation being a replacement of dolomitised and brecciated back-reef carbonates (Pittari, 1999).

The timing of MVT sulphide precipitation is well constrained by a number of techniques. Using carbonate cement stratigraphic relationships in host rock primary porosity, McManus & Wallace (1992) suggested that a single, widespread sulphide precipitation event (pyrite, sphalerite, galena, marcasite) occurred during early burial diagenesis during latest Devonian–earliest Carboniferous time (350 ± 15 Ma) within the reef complexes of the Lennard Shelf. This mineralisation age has since been confirmed by both Rb-Sr dating of sphalerite at Blendevale and U-Pb dating of ore-stage calcites from Goongewa (Wallace et al., 2002). Further south in the basin, the giant saltern evaporite-sealed Admiral Bay Pb-Zn deposit was discovered as part of an oil exploration program, but it is too deep to be exploited by conventional mining techniques McCracken et al., 1997).

Reinforcing the notion of ongoing fault focused fluid evolution controlling mineralisation in the Canning basin are the various stromatolite-baryte-sulphide mounds that constitute outcrops at a number of localities on the eastern Lennard Shelf. They are interpreted as fault-fed synsedimentary exhalative deposits on the Devonian deep basin-margin seafloor (Playford & Wallace, 2001). For example, such stromatolite mounds occur near the Gogo Formation–base Virgin Hills Formation contact and are associated with extensive gossans in outcrop. In drill core, iron sulphides (marcasite and pyrite) are dominant, with base-metal sulphides only occurring as later stage cross-cutting veins.

The varying ore style geometries reflect the simple fact that no bedded evaporites were deposited in the Frasnian-Famennian backreef, only in the Givetian back-shoal region. And so, when the basinal fluid pulses of metalliferous fluids moved up along faults at the basin margin and through the various carbonate hosts, it precipitated well-bedded ore units where metal-carrying fault conduits intersected anhydrites in the Cadjebut Formation and fault/ hydrothermal karst geometries where faults encountered mixtures of hydrocarbons and other reductants in the Frasnian-Famennian platform hosts. Once again, it is clear that dissolving evaporites do not necessarily make ore deposits, when they do, they tend to focus the precipitative process and so make a more concentrated accumulation (Warren, 2016; Chapters 15, 16). As these processes tend to occur in a later digenetic thermal mileu, saddle dolomite is a co-precipitate in many of these evaporite fixed ore deposits.

References

Aitken, J. D., 1981, Stratigraphy and sedimentology of the upper Proterozoic Little Dal Group, Mackenzie Mountains, Northwest Territories: Campbell, F. H. A. Proterozoic basins of Canada. Paper Geological Survey of Canada, v. 10, p. 47-71.

Al Eid, G. A., and A. A. Al Tawil, 2009, Depositional Anhydrite Types and Controls from Anhydrite Cementation within a High-Resolution Sequence Stratigraphic Framework of the Khuff C, Hawiyah Area; Saudi Arabia (Abs.): American Association Petroleum Geologists Search and Discovery Article #90090 ©2009 American Association Petroleum Geologists Annual Convention and Exhibition, Denver, Colorado, June 7–10, 2009

Alonso-Azcarate, J., S. H. Bottrell, and J. Tritlla, 2001, Sulfur redox reactions and formation of native sulfur veins during low grade metamorphism of gypsum evaporites, Cameros Basin (NE Spain): Chemical Geology, v. 174, p. 389-402.

Amrani, A., A. Deev, A. L. Sessions, Y. Tang, J. F. Adkins, R. J. Hill, J. M. Moldowan, and Z. Wei, 2012, The sulfur-isotopic compositions of benzothiophenes and dibenzothiophenes as a proxy for thermochemical sulfate reduction: Geochimica et Cosmochimica Acta, v. 84, p. 152-164.

Biehl, B. C., L. Reuning, J. Schoenherr, V. Lüders, and P. A. Kukla, 2016, Impacts of hydrothermal dolomitization and thermochemical sulfate reduction on secondary porosity creation in deeply buried carbonates: A case study from the Lower Saxony Basin, northwest Germany: Bulletin American Association Petroleum Geologists, v. 100, p. 597-621.

Cai, C., R. H. Worden, S. H. Bottrell, L. S. Wang, and C. C. Yang, 2003, Thermochemical sulphate reduction and the generation of hydrogen sulphide and thiols (mercaptans) in Triassic carbonate reservoirs from the Sichuan Basin, China: Chemical Geology, v. 202, p. 39-57.

Cai, C., Z. Xie, R. H. Worden, G. Hu, L. Wang, and H. He, 2004, Methane-dominated thermochemical sulphate reduction in the Triassic Feixianguan Formation East Sichuan Basin, China: Towards prediction of fatal H2S concentrations: Marine and Petroleum Geology, v. 21, p. 1265-1279.

Cathro, D. L., J. K. Warren, and G. E. Williams, 1992, Halite saltern in the Canning Basin, Western Australia; a sedimentological analysis of drill core from the Ordovician-Silurian Mallowa Salt: Sedimentology, v. 39, p. 983-1002.

Cesaretti, N. N., J. Parnell, and E. A. Dominguez, 2000, Pore fluid evolution within a hydrocarbon reservoir: Yacoraite Formation, (Upper Cretaceous), Northwest Basin, Argentina: Journal of Petroleum Geology, v. 23, p. 375-398.

Davies, G. R., and L. B. Smith, 2006, Structurally controlled hydrothermal dolomite reservoir facies: An overview: Bulletin American Association Petroleum Geologists, v. 90, p. 1641-1690.

Du, Y., T. Fan, H. G. Machel, and Z. Gao, 2018, Genesis of Upper Cambrian-Lower Ordovician dolomites in the Tahe Oilfield, Tarim Basin, NW China: Several limitations from petrology, geochemistry, and fluid inclusions: Marine and Petroleum Geology, v. 91, p. 43-70.

Duggan, J. P., E. W. Mountjoy, and L. D. Stasiuk, 2001, Fault-controlled dolomitization at Swan Hills Simonette oil field (Devonian), deep basin west-central Alberta, Canada: Sedimentology, v. 48, p. 301-323.

Duguid, C., and J. R. Underhill, 2010, Geological controls on Upper Permian Plattendolomit Formation reservoir prospectivity, Wissey Field, UK Southern North Sea: Petroleum Geoscience, v. 16, p. 331-348.

Dworkin, S. I., and L. S. Land, 1994, Petrographic and geochemical constraints on the formation and diagenesis of anhydrite cements, Smackover sandstones, Gulf of Mexico: Journal of Sedimentary Research, Section A: Sedimentary Petrology and Processes, v. 64, p. 339-348.

Ehrenberg, S. N., P. H. Nadeau, and A. A. M. Aqrawi, 2007, A comparison of Khuff and Arab reservoir potential throughout the Middle East: Bulletin American Association Petroleum Geologists, v. 91, p. 275-286.

El Tabakh, M., A. Mory, B. C. Schreiber, and R. Yasin, 2004, Anhydrite cements after dolomitization of shallow marine Silurian carbonates of the Gascoyne Platform, Southern Carnarvon Basin, Western Australia: Sedimentary Geology, v. 164, p. 75-87.

El Tabakh, M., B. C. Schreiber, C. Uthaaroon, L. Coshell, and J. K. Warren, 1998, Diagenetic origin of Basal Anhydrite in the Cretaceous Maha Sarakham Salt - Khorat Plateau, NE Thailand: Sedimentology, v. 45, p. 579-594.

El Tabakh, M., C. Utha-Aroon, J. K. Warren, and B. C. Schreiber, 2003, Origin of dolomites in the Cretaceous Maha Sarakham evaporites of the Khorat Plateau, northeast Thailand: Sedimentary Geology, v. 157, p. 235-252.

Feng, M., P. Wu, Z. Qiang, X. Liu, Y. Duan, and M. Xia, 2017, Hydrothermal dolomite reservoir in the Precambrian Dengying Formation of central Sichuan Basin, Southwestern China: Marine and Petroleum Geology, v. 82, p. 206-219.

Gao, P., G. Liu, G. G. Lash, B. Li, D. Yan, and C. Chen, 2018, Occurrences and origin of reservoir solid bitumen in Sinian Dengying Formation dolomites of the Sichuan Basin, SW China: International Journal of Coal Geology, v. 200, p. 135-152.

Garaguly, I., A. Varga, B. Raucsik, F. Schubert, G. Czuppon, and R. Frei, 2018, Pervasive early diagenetic dolomitization, subsequent hydrothermal alteration, and late stage hydrocarbon accumulation in a Middle Triassic carbonate sequence (Szeged Basin, SE Hungary): Marine and Petroleum Geology, v. 98, p. 270-290.

Gauthier, B. D. M., R. C. W. M. Franssen, and S. Drei, 2000, Fracture networks in Rotliegend gas reservoirs of the Dutch offshore: implications for reservoir behaviour: Geologie en Mijnbouw/Netherlands Journal of Geoscience, v. 79, p. 45-57.

Hao, F., X. Zhang, C. Wang, P. Li, T. Guo, H. Zou, Y. Zhu, J. Liu, and Z. Cai, 2015, The fate of CO2 derived from thermochemical sulfate reduction (TSR) and effect of TSR on carbonate porosity and permeability, Sichuan Basin, China: Earth-Science Reviews, v. 141, p. 154-177.

Heydari, E., 1997, The role of burial diagenesis in hydrocarbon destruction and H2S accumulation, Upper Jurassic Smackover Formation, Black Creek Field, Mississippi: American Association of Petroleum Geologists - Bulletin, v. 81, p. 26-45.

Heydari, E., 2000, Porosity Loss, Fluid Flow, and Mass Transfer in Limestone Reservoirs: Application to the Upper Jurassic Smackover Formation, Mississipi: Bulletin American Association of Petroleum Geologists, p. 1.

Heydari, E., 2010, Dolomites of the Smackover and Buckner Formations in the Mississippi Salt Basin: A Key to Understanding the Dolomitization Process: GCAGS Transactions, v. 60, p. 339-353.

Hips, K., and G. B. Árgyelán, 2007, Controls on diagenesis of the Triassic Kurrachine Dolomite, Syria: GeoArabia, v. 12, p. 41-64.

Hocking, R. M., I. A. Copp, P. E. Playford, and R. H. Kempton, 1996, The Cadjebut Formation: a Givetian evaporitic precursor to Devonian reef complexes of the Lennard Shelf, Canning Basin, Western Australia: Geological Survey of Western Australia, Annual Review, 1995-96, p. 48-55.

Humphrey, E., E. Gomez-Rivas, D. Koehn, P. D. Bons, J. Neilson, J. D. Martín-Martín, and J. Schoenherr, 2019, Stylolite-controlled diagenesis of a mudstone carbonate reservoir: A case study from the Zechstein_2_Carbonate (Central European Basin, NW Germany): Marine and Petroleum Geology, v. 109, p. 88-107.

Jiang, L., C. F. Cai, R. H. Worden, K. K. Li, and L. Xiang, 2013, Reflux dolomitization of the Upper Permian Changxing Formation and the Lower Triassic Feixianguan Formation, NE Sichuan Basin, China: Geofluids, v. 13, p. 232-245.

Jiang, L., R. H. Worden, and C. F. Cai, 2014, Thermochemical sulfate reduction and fluid evolution of the Lower Triassic Feixianguan Formation sour gas reservoirs, northeast Sichuan Basin, China: Bulletin American Association Petroleum Geologists, v. 98, p. 947-973.

Kerans, C., and P. M. Harris, 2008, Devonian Reefal Platforms of the Canning Basin – Lessons Learned and Value as Analogs: AAPG Search and Discovery Article #40302 (2008) - Adapt-

ed from oral presentation at AAPG Annual Convention, Long Beach, CA, April 1-4, 2007.

Krouse, H. R., C. A. Vian, L. S. Eliuk, A. Ueda, and S. Halas, 1988, Chemical and isotopic evidence fo thermochemical sulphate reduction by light hydrocarbon gases in deep carbonate reservoirs: Nature, v. 333, p. 415-419.

Lima, B. E. M., L. R. Tedeschi, A. L. S. Pestilho, R. V. Santos, J. C. Vazquez, J. V. P. Guzzo, and L. F. De Ros, 2019, Deep-burial hydrothermal alteration of the Pre-Salt carbonate reservoirs from northern Campos Basin, offshore Brazil: Evidence from petrography, fluid inclusions, Sr, C and O isotopes: Marine and Petroleum Geology, p. 104143.

Llinas, J. C., 2002, Diagenetic History of the Upper Jurassic Smackover Formation and Its Effects on Reservoir Properties: Vocation Field, Manila Sub-Basin, Eastern Gulf Coastal Plain: Gulf Coast Association of Geological Societies Transactions, v. 52, p. 631-644.

López-Horgue, M. A., E. Iriarte, S. Schröder, P. A. Fernández-Mendiola, B. Caline, H. Corneyllie, J. Frémont, M. Sudrie, and S. Zerti, 2010, Structurally controlled hydrothermal dolomites in Albian carbonates of the Asón valley, Basque Cantabrian Basin, Northern Spain: Marine and Petroleum Geology, v. 27, p. 1069-1092.

López-Quirós, A., M. Barbier, J. M. Martín, and X. Guichet, 2018, Sedimentology and diagenetic evolution of the Neogene 'Intermediate Sandstone Unit' in the halite deposits of the Granada Basin (SE Spain): the turning point in the change from marine to continental sedimentation: Journal of Iberian Geology, v. 44, p. 513-537.

Loucks, R. G., 1999, Paleocave carbonate reservoirs: origins, burial-depth modifications, spatial complexity, and reservoir implications: American Association of Petroleum Geologists, v. 83, p. 1795-1834.

Luczaj, J. A., and R. H. Goldstein, 2000, Diagenesis of the lower Permian Krider member, southwest Kansas, USA: Fluid-inclusion, U-Pb, and fission-track evidence for reflux dolomitization during latest Permian time: Journal of Sedimentary Research Section A-Sedimentary Petrology & Processes, v. 70, p. 762-773.

Lynch, G., and P. S. Giles, 1996, The Ainslie Detachment: a regional flat-lying extensional fault in the Carboniferous evaporitic Maritimes Basin of Nova Scotia, Canada: Canadian Journal of Earth Sciences, v. 33, p. 169-181.

Machel, H. G., 2001, Bacterial and thermochemical sulfate reduction in diagenetic settings - old and new insights: Sedimentary Geology, v. 140, p. 143-175.

Machel, H. G., 2013, Secondary anhydrites in deeply buried Devonian carbonates of the Alberta Basin, Canada: Carbonates and Evaporites, p. 1-14.

McCracken, S. R., H. Etminan, A. G. Connor, and V. A. Williams, 1997, Geology of the Admiral Bay carbonate-hosted zinc-lead deposit, Canning Basin, Western Australia: Special Publication - Society of Economic Geologists, v. 4, p. 330-349.

Meilijson, A., J. Steinberg, F. Hilgen, F. Bialik, F. Waldmann, and Y. Makovsky, 2018, Deep-basin evidence resolves a 50-year-old debate and demonstrates synchronous onset of Messinian evaporite deposition in a non-desiccated Mediterranean: Geology, v. 46, p. 243-246.

Moore, C. H., and W. J. Wade, 2009, Carbonate Reservoirs (2nd Edition); Porosity and diagenesis in a sequence stratigraphic framework, Elsevier, 392 p.

Morad, D., F. H. Nader, S. Morad, C. Rossi, M. Gasparrini, M. Alsuwaidi, F. Al Darmaki, and H. Hellevang, 2019, Limited thermochemical sulfate reduction in hot, anhydritic, sour gas carbonate reservoirs: The Upper Jurassic Arab Formation, United Arab Emirates: Marine and Petroleum Geology, v. 106, p. 30-41.

Morley, C. K., 2012, Late Cretaceous-Early Palaeogene tectonic development of SE Asia: Earth-Science Reviews, v. 115, p. 37-75.

Morrow, D. W., M. Zhao, and L. D. Stasiuk, 2002, The gas-bearing Devonian Presqu'ile Dolomite of the Cordova embayment region of British Columbia, Canada: Dolomitization and the stratigraphic template: Bulletin American Association of Petroleum Geologists, v. 86, p. 1609-1638.

Navarro-Ciurana, D., M. Corbella, E. Cardellach, E. Vindel, D. Gómez-Gras, and A. Griera, 2016, Petrography and geochemistry of fault-controlled hydrothermal dolomites in the Riópar area (Prebetic Zone, SE Spain): Marine and Petroleum Geology, v. 71, p. 310-328.

North, F. K., 1990, Petroleum Geology. Second Ed.: Winchester, Mass, Unwin Hyman Ltd, 631 p.

Okere, D., and S. Toothill, 2012, New insights into hydrocarbon plays in the Caspian Sea, Kazakhstan: Petroleum Geoscience, v. 18, p. 253-268.

Pittari, A., 1999, Geology of the Kutarta zinc-lead deposit, Lennard Shelf, Western Australia.: Honours Thesis, University of Melbourne, Department of Earth Sciences, unpublished.

Playford, P. E., and M. W. Wallace, 2001, Exhalative Mineralization in Devonian Reef Complexes of the Canning Basin, Western Australia: Economic Geology, v. 96, p. 1595-1610.

Presley, M. W., 1987, Evolution of Permian evaporite basin in Texas Panhandle: AAPG Bulletin, v. 71, p. 167-190.

Radke, B. M., and R. L. Mathis, 1980, On the formation and occurrence of saddle dolomite: Journal of Sedimentary Petrology, v. 50, p. 1149-1168.

Ren, Q., Y. Du, D. Gao, B. Li, X. Zhang, X. Liu, and X. Yuan, 2018, A Multi–fluid Constrain for the Forming of Potash Deposits in the Savannakhet Basin: Geochemical Evidence from

Halite: Acta Geologica Sinica, v. 92, p. 755-768.

Rosell, O. L., and C. F. Orti, 1980, Presencia de analcima y observaciones diageneticas en la anhidrita basal de la cuenca potasica de Navarra (Eocene superior, Cuenca del Ebro, Espana): Lectures and communications from the First symposium on diagenesis of sediments and sedimentary rocks. Univ. Barcelona, Dep. Petrol. y Geoquim., Barcelona, Spain. Revista del Instituto de Investigaciones Geologicas de la Diputacion Provincial de Barcelona, v. 34, p. 223-235.

Saller, A. H., B. Ball, S. S. Robertson, B. McPherson, C. Wene, R. Nims, and J. Gogas, 2001, Reservoir characteristics of Devonian cherts and their control on oil recovery: Dollarhide field, west Texas: Bulletin American Association Petroleum Geologists, v. 85, p. 35-50.

Spötl, C., and J. K. Pitman, 1998, Saddle (Baroque) Dolomite in Carbonates and Sandstones: A Reappraisal of a Burial-Diagenetic Concept: Carbonate Cementation in Sandstones, p. 437-460.

Spötl, C., and J. K. Pitman, 1998, Saddle (Baroque) Dolomite in Carbonates and Sandstones: A Reappraisal of a Burial-Diagenetic Concept: Carbonate Cementation in Sandstones, p. 437-460.

Sullivan, M. D., R. S. Haszeldine, A. J. Boyce, G. Rogers, and A. E. Fallick, 1994, Late anhydrite cements mark basin inversion; isotopic and formation water evidence, Rotliegend Sandstone, North Sea: Marine and Petroleum Geology, v. 11, p. 46-54.

Swennen, R., V. Vandeginste, and R. Ellam, 2003, Genesis of zebra dolomites (Cathedral Formation: Canadian Cordillera Fold and Thrust Belt, British Columbia): Journal of Geochemical Exploration, v. 78-79, p. 571-577.

Tompkins, L. A., V. A. Pedone, M. T. Roche, and D. I. Groves, 1994a, The Cadjebut deposit as an example of Mississippi Valley-Type mineralization on the Lennard Shelf, Western Australia - Single episode or multiple events: Economic Geology, v. 89, p. 450-466.

Tompkins, L. A., M. J. Rayner, D. I. Groves, and M. T. Roche, 1994b, Evaporites; in situ sulfur source for rhythmically banded ore in the Cadjebut mississippi valley-type Zn-Pb deposit, Western Australia: Economic Geology, v. 89, p. 467-492.

Trudinger, P. A., L. A. Chambers, and J. W. Smith, 1985, Low-temperature sulphate reduction; biological versus abiological: Canadian Journal of Earth Sciences, v. 22, p. 1910-1918.

Wallace, M. W., H. A. Middleton, B. Johns, and S. Marshallsea, 2002, Hydrocarbons and Mississippi Valley-type sulfides in the Devonian reef complexes of the eastern Lennard Shelf, Canning Basin, Western Australia: The sedimentary basins of Western Australia 3. Proceedings of the West Australian basins Symposium: Perth, Petroleum Exploration Society of Australia, p. 795-815.

Wallace, M. W., H. Moxham, B. Johns, and S. Marshallsea, 1997, Burial Dolomitization, Mississippi Valley-type Mineralization and Hydrocarbon Generation in the Devonian Reef Complexes of the Lennard Shelf, Canning Basin, Western Australia: Sedimentary Events, Hydrocarbon Systems - CSPG-SEPM Joint Convention: Program with Abstracts, p. 288-288.

Warren, J. K., 2000, Dolomite: Occurrence, evolution and economically important associations: Earth Science Reviews, v. 52, p. 1-81.

Warren, J. K., 2016, Evaporites: A compendium (ISBN 978-3-319-13511-3): Berlin, Springer, 1854 p.

Wei, A., C. Xue, K. Xiang, J. Li, C. Liao, and Q. J. Akhter, 2015, The ore-forming process of the Maoping Pb–Zn deposit, northeastern Yunnan, China: Constraints from cathodoluminescence (CL) petrography of hydrothermal dolomite: Ore Geology Reviews, v. 70, p. 562-577.

Wendte, J., H. R. Qing, J. J. Dravis, S. L. O. Moore, L. D. Stasiuk, and G. Ward, 1998, High temperature saline (thermoflux) dolomitisation of Devonian Swan Hills platform and bank carbonates, Wild River area, west-central Alberta: Bulletin of Canadian Petroleum Geology, v. 46, p. 210-265.

Williams, G. K., 1984, Some musings on the Devonian Elk Point Basin, western Canada: Bulletin of Canadian Petroleum Geology, v. 32, p. 216-232.

Winter, B. L., C. M. Johnson, J. A. Simo, and J. W. Valley, 1995, Paleozoic fluid history of the Michigan basin - evidence from dolomite geochemistry in the Middle Ordovician St Peter Sandstone: Journal of Sedimentary Research Section A-Sedimentary Petrology & Processes, v. 65, p. 306-320.

Worden, R. H., and P. C. Smalley, 1996, H2S-Producing reactions in deep carbonate gas reservoirs - Khuff Formation, Abu Dhabi: Chemical Geology, v. 133, p. 157-171.

Worden, R. H., P. C. Smalley, and M. M. Cross, 2000, The influence of rock fabric and mineralogy on thermochemical sulfate reduction: Khuff Formation, Abu Dhabi: Journal of Sedimentary Research Section A-Sedimentary Petrology & Processes, v. 70, p. 1210-1221.

Worden, R. H., P. C. Smalley, and N. H. Oxtoby, 1995, Gas souring by thermochemical sulfate reduction at 140° C: American Association of Petroleum Geologists Bulletin, v. 79, p. 854-863.

Worden, R. H., P. C. Smalley, and N. H. Oxtoby, 1995, Gas souring by thermochemical sulfate reduction at 140° C: American Association of Petroleum Geologists Bulletin, v. 79, p. 854-863.

Yang, C., I. Hutcheon, and H. R. Krouse, 2001, Fluid inclusion and stable isotope studies of thermochemical sulphate reduction from Burnt Timber and Crossfield East gas fields in Alberta, Canada: Bulletin of Canadian Petroleum Geology, v. 49, p. 149-164.

Zhang, P., G. Liu, C. Cai, M. Li, R. Chen, P. Gao, C. Xu, W. Wan, Y. Zhang, and M. Jiang, 2019, Alteration of solid bitumen by hydrothermal heating and thermochemical sulfate reduction in the Ediacaran and Cambrian dolomite reservoirs in the Central Sichuan Basin, SW China: Precambrian Research, v. 321, p.

277-302.

Zhu, G., T. Wang, Z. Xie, B. Xie, and K. Liu, 2015, Giant gas discovery in the Precambrian deeply buried reservoirs in the Sichuan Basin, China: Implications for gas exploration in old cratonic basins: Precambrian Research, v. 262, p. 45-66.

Zhu, G., T. Wang, Z. Xie, B. Xie, and K. Liu, 2015, Giant gas discovery in the Precambrian deeply buried reservoirs in the Sichuan Basin, China: Implications for gas exploration in old cratonic basins: Precambrian Research, v. 262, p. 45-66.

Saltworks Consultants Pty Ltd
ABN 068 889 127
Kingston Park,
5049 South Australia

Email: enquiries@saltworkconsultants.com

Web Page: www.saltworkconsultants.com